Modulation of FAK and Src adhesion signaling occurs independently of adhesion complex composition

Edward R. Horton,[1] Jonathan D. Humphries,[1] Ben Stutchbury,[1] Guillaume Jacquemet,[1] Christoph Ballestrem,[1] Simon T. Barry,[2] and Martin J. Humphries[1]

[1]Wellcome Trust Centre for Cell-Matrix Research, Faculty of Life Sciences, University of Manchester, Manchester M13 9PT, England, UK
[2]Oncology iMed, AstraZeneca, Cheshire SK10 4TG, England, UK

Integrin adhesion complexes (IACs) form mechanochemical connections between the extracellular matrix and actin cytoskeleton and mediate phenotypic responses via posttranslational modifications. Here, we investigate the modularity and robustness of the IAC network to pharmacological perturbation of the key IAC signaling components focal adhesion kinase (FAK) and Src. FAK inhibition using AZ13256675 blocked FAK^{Y397} phosphorylation but did not alter IAC composition, as reported by mass spectrometry. IAC composition was also insensitive to Src inhibition using AZD0530 alone or in combination with FAK inhibition. In contrast, kinase inhibition substantially reduced phosphorylation within IACs, cell migration and proliferation. Furthermore using fluorescence recovery after photobleaching, we found that FAK inhibition increased the exchange rate of a phosphotyrosine (pY) reporter (dSH2) at IACs. These data demonstrate that kinase-dependent signal propagation through IACs is independent of gross changes in IAC composition. Together, these findings demonstrate a general separation between the composition of IACs and their ability to relay pY-dependent signals.

Introduction

Cell adhesion to the ECM is mediated by cell surface receptors including integrins (Juliano, 2002; Morgan et al., 2007). Upon integrin–ECM engagement and integrin clustering, proteins are recruited to form multimolecular integrin adhesion complexes (IACs) that facilitate the linkage between integrins and the actin cytoskeleton (Brakebusch and Fässler, 2003). Positioned between the ECM and the actin cytoskeleton, IACs permit bidirectional signaling and transmission of mechanical force across the plasma membrane (Evans and Calderwood, 2007; Oakes et al., 2012; Hu and Luo, 2013). Over 200 components localize to IACs as reported in the literature-curated integrin adhesome (Zaidel-Bar et al., 2007; Winograd-Katz et al., 2014). Adaptors and actin regulators act as scaffolding molecules, whereas a large number of signaling molecules influence several downstream biological functions and contribute to diseases such as developmental and cardiovascular disorders, inflammation, and cancer (Wahl et al., 1996; Mitra and Schlaepfer, 2006; Winograd-Katz et al., 2014; Maartens and Brown, 2015).

Phosphorylation is a posttranslational modification that has been widely implicated in the regulation of adhesion signaling and dynamics (Zaidel-Bar and Geiger, 2010). Imaging cells with generic anti-phosphotyrosine (pY) antibodies or fluorescent proteins tagged to the Src homology 2 (SH2) domain of Src demonstrated an enrichment of pY events at IACs (Kirchner et al., 2003; Ballestrem et al., 2006), and phosphoproteomics has identified numerous phosphorylation sites at IACs (Robertson et al., 2015) or that are stimulated by adhesion (Chen et al., 2009; Schiller et al., 2013). Focal adhesion kinase (FAK), an extensively tyrosine-phosphorylated protein, is a core component of IACs (Horton et al., 2015a) and is one of the earliest recruited IAC components (Kornberg et al., 1992; Schaller et al., 1992). FAK regulates cell migration and IAC dynamics, as FAK recruits talin to newly formed IACs (Lawson et al., 2012) and FAK-null cells display reduced rates of IAC turnover (Ilić et al., 1995; Webb et al., 2004; Ezratty et al., 2005; Chan et al., 2010). After cell–ECM engagement, FAK autophosphorylation at FAK^{Y397} exposes an SH2 domain-binding site for Src (Schaller et al., 1994). Src recruitment results in Src-dependent phosphorylation of FAK at FAK^{Y576} and FAK^{Y577} leading to maximal adhesion-induced FAK activation (Calalb et al., 1995). FAK and Src are two of the most connected adhesome components (Zaidel-Bar et al., 2007), and the FAK–Src signaling complex, which is a potential therapeutic target in cancer (Brunton and Frame, 2008; Kim et al., 2009; Sulzmaier et al., 2014), binds to and phosphorylates other IAC molecules

Correspondence to Martin J. Humphries: martin.humphries@manchester.ac.uk

E.R. Horton's present address is Biotech Research and Innovation Centre, University of Copenhagen, Copenhagen DK-2200, Denmark.

G. Jacquemet's present address is Turku Centre for Biotechnology, University of Turku, 20520 Turku, Finland.

Abbreviations used in this paper: ACN, acetonitrile; FA, formic acid; FAK [i], FAK inhibitor AZ13256675; FN, fibronectin; HFF, human foreskin fibroblast; IAC, integrin adhesion complex; MF, mobile fraction; MS, mass spectrometry; PF228, PF-573,228; PF271, PF-562,271; pY, phosphotyrosine; SH2, Src homology 2; Src [i], Src inhibitor AZD0530; Tf, transferrin.

The Rockefeller University Press $30.00
J. Cell Biol. Vol. 212 No. 3 349–364
www.jcb.org/cgi/doi/10.1083/jcb.201508080

such as paxillin and p130Cas (Schaller and Parsons, 1995; Mitra and Schlaepfer, 2006).

To provide global insights into IAC biology, recent studies have isolated IACs biochemically and analyzed their molecular composition using mass spectrometry (MS)–based proteomics (Kuo et al., 2012; Jones et al., 2015). These studies have revealed an unanticipated complexity in IAC composition in different contexts (Humphries et al., 2009; Kuo et al., 2011; Schiller et al., 2011, 2013; Byron et al., 2012, 2015; Huang et al., 2014; Ng et al., 2014; Yue et al., 2014; Ajeian et al., 2015; Robertson et al., 2015; Horton et al., 2015a). In particular, analysis of the effects of myosin-II inhibition on IAC composition revealed the force-sensitive nature of LIN-11, Isl1, and MEC-3 domain–containing IAC components (Kuo et al., 2011; Schiller et al., 2011; Horton et al., 2015a,b). Using complementary advanced microscopy approaches (Humphries et al., 2015), it has been shown that components are recruited to IACs as preformed complexes (Bachir et al., 2014; Hoffmann et al., 2014). These studies support a view that IACs may be organized into modular substructural units (Zaidel-Bar et al., 2007; Byron et al., 2010). Here, we sought to examine further the modular nature of the adhesome and investigate the sensitivity of the IAC network to perturbation. Rather than reducing protein expression levels to inhibit scaffolding and signaling functional roles, we specifically targeted the catalytic activity of the key IAC signaling kinases FAK and Src (Zaidel-Bar et al., 2007). Using pharmacological inhibitors and a combination of targeted and global approaches, we demonstrate that IAC protein composition and dynamics were largely unaffected by kinase inhibition, highlighting the robustness of the IAC network to FAK and Src kinase perturbation. In contrast, pY levels of IAC proteins and thus adhesion signaling, cell migration, and proliferation were reduced, and the dynamics of a pY reporter were increased, upon kinase inhibition. These data demonstrate that kinase activity at key IAC hubs regulates adhesion signaling and information flux through IACs but is not required to maintain IAC composition, suggesting a separation in the regulation of the structural and signaling contributions of IAC components to control adhesion-dependent cellular functions.

Results

Inhibition of FAK activity using the small-molecule inhibitor AZ13256675

To inhibit FAK activity, we explored the inhibitory properties of the small-molecule FAK inhibitor AZ13256675 (FAK [i]). To determine a concentration of FAK inhibitor required to inhibit FAK catalytic activity in cells, human foreskin fibroblasts (HFFs) were plated on fibronectin (FN)-coated dishes for 1 h and then treated with half-log dilutions of FAK [i] for 1 h. Using the FAK autophosphorylation residue FAK^{Y397} to assess FAK catalytic activity, a dose-dependent reduction in FAK^{Y397} was observed in FAK [i]–treated cells (Fig. 1 A). Maximal inhibition (87%) of FAK^{Y397} levels was obtained at 3 µM FAK [i] (Fig. 1, A, B, and D), which was equivalent to FAK^{Y397} levels from cells kept in suspension and was similar to FAK inhibition reported by others (Slack-Davis et al., 2007; Tanjoni et al., 2010; Stokes et al., 2011). In contrast, treating cells with 3 µM FAK [i] resulted in only 37% inhibition of the Src-substrate site FAK^{Y576} (Fig. 1 C), indicating the specificity of FAK [i] for FAK^{Y397}. In addition, a dose-dependent reduction of FAK^{Y397} levels was observed in cells treated with FAK [i] by immunofluorescence (Fig. 1, E and F). In a recombinant kinase assay, FAK [i] and a commonly used FAK inhibitor, PF-562,271 (PF271; Stokes et al., 2011), inhibited FAK^{Y397} phosphorylation with an IC_{50} of 4.3 and 5.6 nM, respectively. In a parallel cell-based assay using HEK293 cells, FAK [i] and PF271 inhibited FAK^{Y397} phosphorylation with an IC_{50} of 40 and 49 nM, respectively. These data demonstrate that FAK [i] and PF271 showed similar potency against FAK. To assess selectivity, both FAK [i] and PF271 were screened against a panel of recombinant enzymes (Table S1; Davies et al., 2000; Bain et al., 2003). FAK [i] was selective against the majority of kinases tested and showed improved selectivity against FAK compared with PF271 (Table S1). These data indicate that FAK [i] is a potent and selective inhibitor of the phosphorylation of FAK^{Y397}.

In contrast to FAK^{Y397}, the cell area covered by vinculin-containing IACs and the actin cytoskeleton were unchanged upon FAK inhibition (Fig. 1, E and G). To confirm these effects using an alternative FAK inhibitor, we compared the effects of treating HFF cells prespread on FN with FAK [i] or the established FAK inhibitor PF-573,228 (PF228; Slack-Davis et al., 2007; Fig. 1, H and I). FAK^{Y397} was significantly reduced upon treatment with either compound, and there was an equivalent reduction in FAK^{Y397} levels between cells treated with FAK [i] or PF228 (Fig. 1 J). In contrast, both the area and numbers of vinculin- or paxillin-containing IACs, and the actin cytoskeleton, were unaffected by treatment with both inhibitors (Fig. 1, K–M). In summary, these data indicate that treatment with 3 µM FAK [i] reduces FAK^{Y397} levels in cells to the same extent as commonly used FAK inhibitors while having no effect on vinculin- or paxillin-containing IACs.

IAC composition is robust to FAK inhibition

To determine global effects of FAK inhibition on IAC composition in an unbiased manner, a proteomics workflow was used to define the composition of FN-induced IACs isolated from cells treated with FAK [i] (Fig. 2 A). To assess proteins specifically recruited to FN, complexes were also isolated from cells plated on the negative control ligand transferrin (Tf), which allows integrin-independent cell attachment via the Tf receptor (Jones et al., 2015; Robertson et al., 2015). A similar level of total protein was collected between cells treated with DMSO or FAK [i] (Fig. 2 B) and immunoblotting of isolated complexes with antibodies directed against canonical IAC proteins (vinculin, integrin-linked kinase [ILK], paxillin, and filamin A) and non-IAC components (Tf receptor and the mitochondrial protein BAK) demonstrated the enrichment of IAC proteins compared with the Tf control (Fig. 2 C). To allow the global quantitative comparison of IAC composition, isolated FN-induced IACs were analyzed by MS using a label-free intensity-based approach for relative protein quantification. In total, 898 proteins were identified and quantified with a minimum of two unique peptides per protein (Fig. 2 D and Table S2), which included many canonical IAC components (e.g., talin, vinculin, ILK, paxillin, FAK, and the FN-binding integrins α5β1 and αVβ3). To interrogate the dataset further, comparisons were performed with three different measures of IAC composition: the meta-adhesome (Horton et al., 2015a), which contains 2,412 proteins identified in at least one of seven previously published FN-induced IAC MS datasets; the literature-curated adhesome (Winograd-Katz et al., 2014), which contains 232 proteins reported to localize

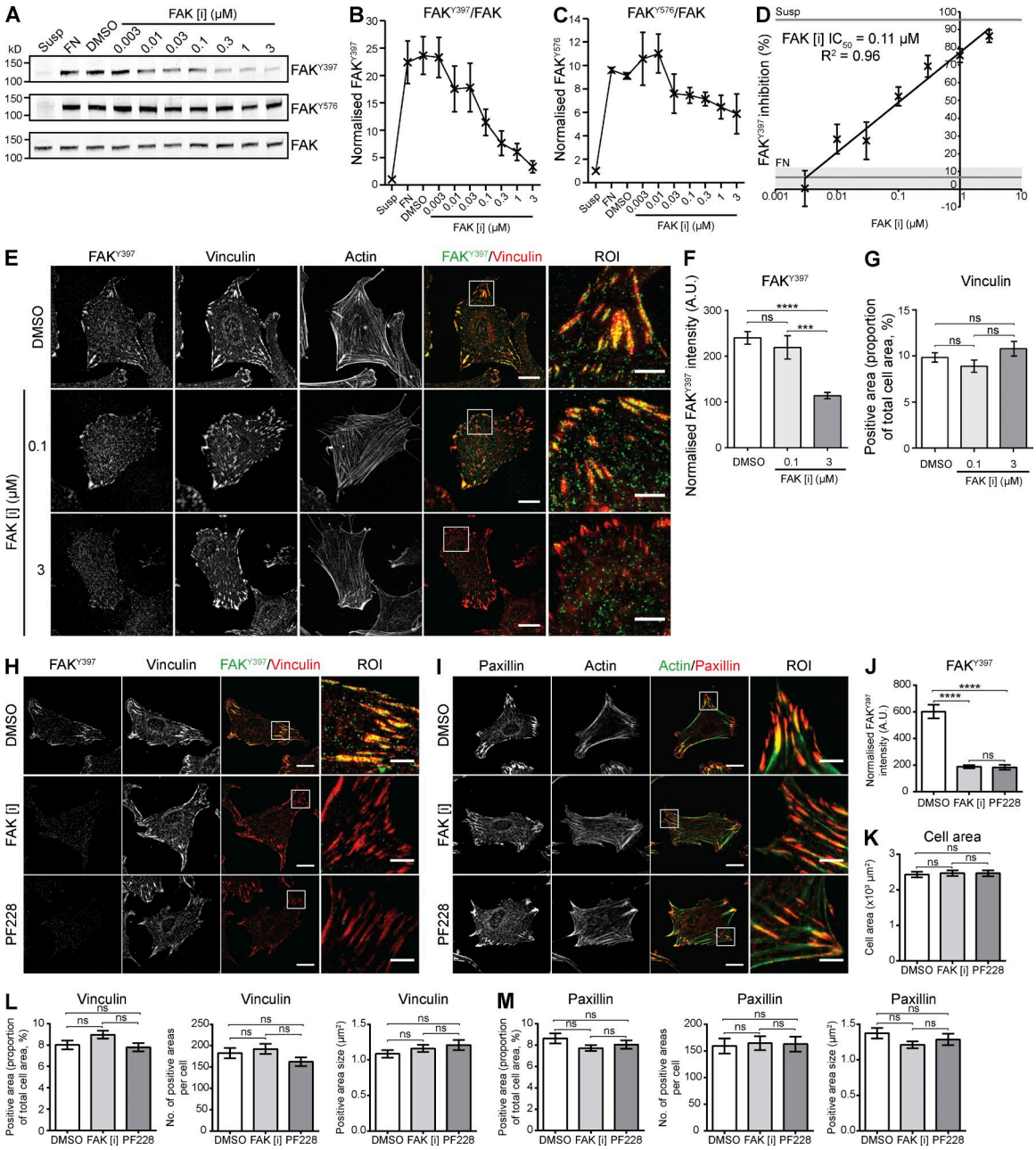

Figure 1. **Inhibition of FAK activity by FAK [i] in human fibroblasts.** (A) Immunoblotting of FAK phosphorylation sites FAK^{Y397} and FAK^{Y576} and total FAK in total cell lysates. HFF cells spread on FN for 1 h were treated with DMSO or the FAK inhibitor AZ13256675 (FAK [i]) for 1 h using half-log dilutions. Cells kept in suspension for 30 min (Susp) were used to detect basal FAK activity. Untreated cells spread on FN for 2 h were used to detect maximal FAK activity. FAK^{Y397} and FAK^{Y576} were used to assess FAK catalytic activity. Molecular mass values (kD) are displayed. (B and C) Quantification of immunoblotted membranes in A. FAK phosphorylation values FAK^{Y397} (B) and FAK^{Y576} (C) were normalized to total FAK (mean ± SEM, $n = 3$). (D) Dose–response curve using FAK^{Y397} as a readout for FAK activity to determine percentage inhibition relative to cells treated with DMSO. Gray lines and shading show values for suspension and untreated FN conditions (not used to calculate the trendline, mean ± SEM, $n = 3$). The 50% FAK^{Y397} inhibitory concentration (IC_{50}) was calculated as 0.11 µM FAK [i] using the formula $y = 12.23\ln(x) + 76.99$ (y, percentage inhibition; x, FAK [i] concentration). (E) HFFs spread on FN for 1 h were treated with DMSO, 0.1 µM FAK [i], or 3 µM FAK [i] for 1 h. IACs were visualized by staining for FAK^{Y397} (green) and vinculin (red) by immunofluorescence. The actin cytoskeleton was visualized by staining with fluorophore-conjugated phalloidin. Bars: (main) 20 µm; (ROI) 5 µm. (F and G) Quantification of FAK^{Y397} pixel intensity in vinculin-positive areas (F) and the cell area covered by vinculin-positive areas (G). In F, FAK^{Y397} intensity values were normalized to the proportion of the cell area covered by vinculin-positive areas (mean ± SEM, $n > 20$ cells). (H and I) HFFs spread on FN for 1 h were treated with DMSO, 3 µM FAK [i] or 10 µM PF228 for 1 h. IACs were visualized by staining for FAK^{Y397} (green) and vinculin (red; H) or paxillin (red; I) by immunofluorescence. In I, the actin cytoskeleton was visualized by staining with fluorophore-conjugated phalloidin (green). Bars: (main) 20 µm; (ROI) 5 µm. (J–M) Quantification of images in H and I. Graphs show quantification of FAK^{Y397} pixel intensity in vinculin-positive areas (J) and the total cell area (K). Vinculin (L) and paxillin (M) were quantified by the cell area covered by positive staining of the indicated protein, the number of positive areas measured per cell and the mean positive area size. In J, FAK^{Y397} intensity values were normalized to the proportion of the cell area covered by vinculin-positive areas. Graphs show mean ± SEM, $n \geq 15$ cells. ***, $P < 0.001$; ****, $P < 0.0001$; ns, not significant; Kruskal–Wallis test with Dunn's post hoc correction. A.U., arbitrary units. Representative images are shown.

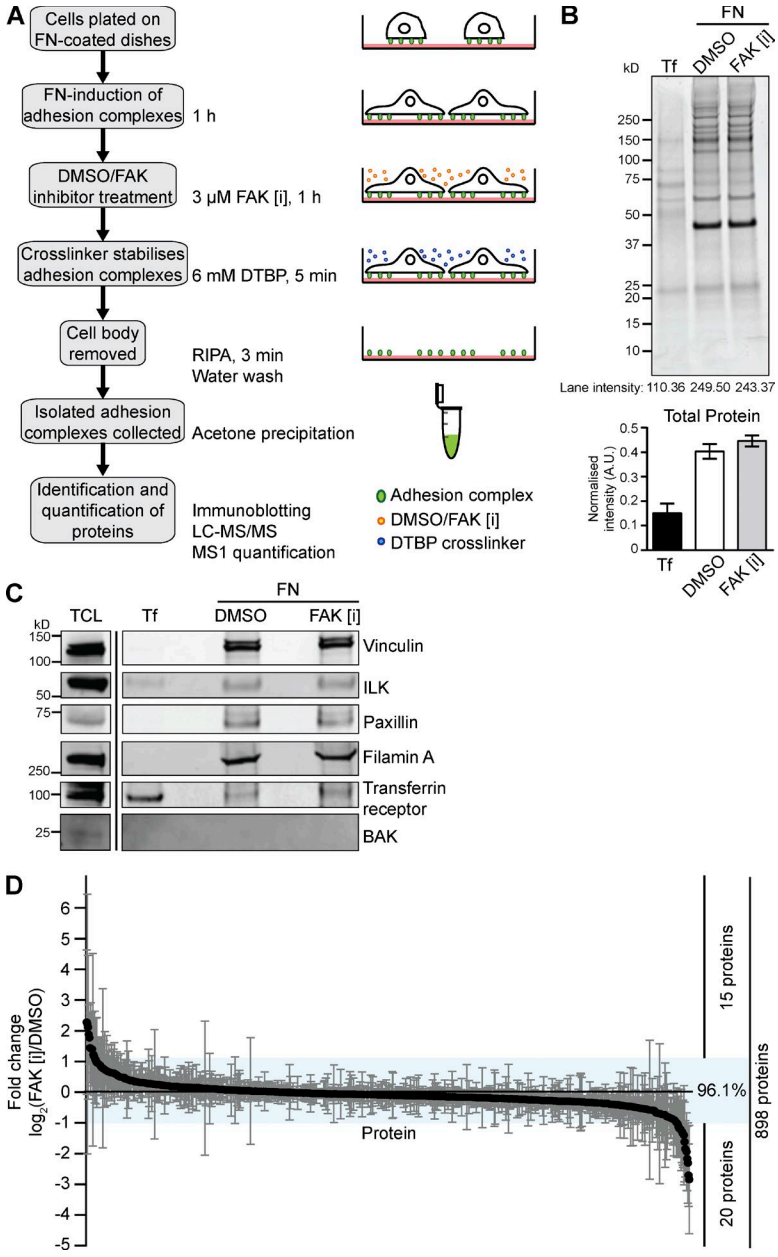

Figure 2. **Effects of FAK inhibition on IAC composition.** (A) IACs were isolated from HFF cells spread on FN for 1 h followed by treatment with DMSO or 3 µM FAK [i] for 1 h using the workflow shown (see Materials and methods). (B and C) Isolated IACs were analyzed by SDS-PAGE (B) and immunoblotting (C). Representative total protein intensity values for each lane are indicated. Graph shows intensity values normalized to the summed intensities in each experiment (mean ± SEM, $n = 3$). Complexes isolated from cells spread on Tf and cell lysates from cells spread on FN (TCL) were used as negative and positive controls, respectively. Molecular mass values (kD) are displayed. Representative images are shown. (D) Isolated IACs were analyzed by MS. Using an intensity-based quantification approach, 898 proteins were identified and quantified satisfying at least two unique peptides per protein (Table S2). Graph shows ratios of normalized intensity values ($\log_2$(FAK [i]/DMSO), mean ± SEM, $n = 3$) for each protein. Blue shading corresponds to ≤twofold change between conditions (863 proteins, 96.1% of dataset). In total, 15 and 20 proteins increased and decreased, respectively, upon FAK inhibition by at least twofold. LC-MS/MS, liquid chromatography tandem MS.

to IACs; and the consensus adhesome (Horton et al., 2015a), which contains 60 proteins that are most robustly identified in FN-induced IAC MS datasets. In total, 617 meta-adhesome proteins (69% of dataset; 25% of meta-adhesome; Fig. S1 A), 75 literature-curated adhesome proteins (8% of dataset; 31% of literature-curated adhesome; Fig. S1 B), and 49 consensus adhesome proteins (5% of dataset; 82% of consensus adhesome; Fig. S1 C) were identified in IACs isolated from cells treated with DMSO and FAK [i], which is of a similar scale and coverage to other MS-derived IAC datasets (Horton et al., 2015a). These data confirmed the successful identification of IAC components in this dataset.

To quantify compositional changes in IACs upon FAK inhibition, intensity values were normalized to total protein amount and the mean fold change between DMSO and FAK [i] conditions was determined for each protein (Table S2 and Fig. 2 D). Surprisingly, most proteins identified (863, 96%) changed in abundance by less than twofold upon FAK inhibition (Fig. 2 D and Table S2), which is in contrast to the myosin-II–responsive IAC proteome, where over half of IAC components were affected upon blebbistatin treatment using the same cell type (Kuo et al., 2011). In addition, all 49/60 consensus adhesome proteins identified (Horton et al., 2015a) changed in abundance by less than 1.4-fold upon FAK inhibition (Fig. S1 C). This is in contrast to changes in consensus adhesome proteins upon blebbistatin treatment in three other studies (mean 1.1-fold decrease upon FAK inhibition vs. 2.1-fold decrease upon blebbistatin treatment; Horton et al., 2015b). Only 35 proteins changed in abundance by at least twofold upon FAK inhibition (Fig. 2 D); however, only two proteins, which have not been linked to adhesion in the past, showed small but significant ($P < 0.05$) changes upon FAK inhibition (RRBP1, 1.46-fold decrease; CRYL1, 1.31-fold increase; Table S2). The majority of proteins identified changed in abundance by less than twofold relative to vinculin (856, 95%; Table S3), indicating that the lack of changes observed were not caused by

the normalization approach. To examine proteins located in the vicinity of FAK and integrins in IACs, we performed protein–protein interaction network analysis and found that the majority of proteins identified that were reported to bind to FAK or β1 integrin were insensitive to FAK inhibition, although small, nonsignificant differences in the SH2 domain–containing kinase YES1 (1.76-fold increase) and the phosphatase PTPN11 (1.65-fold decrease) were identified (Fig. S1 D and Table S2). In summary, these data suggest that IAC protein composition is largely unaffected by a reduction in FAK^{Y397}.

The duration and timing of FAK inhibition does not affect IAC formation and cell adhesion

To examine further the effect of FAK inhibition on IAC composition, the actin cytoskeleton, and cell adhesion, we tested whether there were time-dependent changes in IACs or defects in cell spreading or adhesion maturation upon FAK inhibition. To examine the effects of FAK inhibition on IAC maturation, preadherent HFF cells were treated with FAK [i] for 1–4 h (Figs. 3, A and B; and Fig. S2 A) or for 16 h (Figs. 3, C and D; and Fig. S2 B, Adh). To examine the effects of FAK inhibition on cell spreading and IAC formation, FAK [i] was added to cells kept in suspension before FN attachment (Figs. 3, C and D; and Fig. S2 B, Susp). Cells attached to FN-coated plates formed IACs and displayed no actin cytoskeletal, cell morphological, or cell spreading defects in all conditions tested (Figs. 3 and S2). Although treating cells with FAK [i] significantly reduced FAK^{Y397}-positive areas in all conditions (Fig. 3), there were no significant effects on the cell area covered by vinculin- and paxillin-containing IACs (Figs. 3 and S2). In summary, these data support the MS findings and suggest that FAK^{Y397} is not required for cell attachment, cell spreading, or the formation or maintenance of FN-induced vinculin- or paxillin-containing IACs.

Cell migration and proliferation are sensitive to FAK and Src inhibition

To confirm FAK inhibition upon treatment with FAK [i] functionally, we examined previously reported outputs of FAK and Src signaling: cell migration (Ilić et al., 1995; Sieg et al., 1999; Slack et al., 2001) and proliferation (Gilmore and Romer, 1996; Sánchez-Bailón et al., 2012; Serrels et al., 2012; Luo et al., 2013; Je et al., 2014). Because FAK and Src form a signaling complex and have overlapping functions (Mitra and Schlaepfer, 2006), we also perturbed the function of Src using the small-molecule Src kinase inhibitor AZD0530/saracatinib (Src [i]; Plé et al., 2004; Hennequin et al., 2006). To determine the concentration of Src [i] required to inhibit Src catalytic activity effectively, HFF cells were plated on FN-coated dishes and treated with half-log dilutions of Src [i] for 1 h. Immunoblotting demonstrated a dose-dependent reduction in the Src substrate paxillin^{Y118} (Serrels et al., 2006) and the Src activation site Src^{Y416} in Src [i]–treated cells, and maximum inhibition was obtained at 3 µM Src [i] (Fig. S3).

To examine the effect of FAK and/or Src inhibition on cell migration, cells were treated with inhibitors in scratch wound assays (Fig. 4, A–C). Cells migrated into wounded monolayers in all conditions tested, but migration distance and speed were reduced in inhibitor-treated cells, particularly for cells treated with Src [i] and combined FAK [i] and Src [i] (Fig. 4, B and C).

To investigate the effect of FAK and/or Src inhibition on cell proliferation, cells were incubated in the presence of DMSO or inhibitors for up to 4 d and total cell number measured (Fig. 4 D). Cells proliferated in all conditions tested; however, the increase in cell number was reduced in cells treated with inhibitors (inhibition of proliferation relative to DMSO; FAK [i], 43%; Src [i], 30%; FAK [i] and Src [i], 67%; Fig. 4 D). To confirm the differences seen in cell proliferation, we investigated the effects of inhibitor treatment on DNA synthesis as measured by EdU incorporation. Serum starvation was used to induce cell cycle arrest in cells and was used as a negative control. The proportion of actively dividing cells was 26% in cells treated with DMSO, which was reduced in cells treated with FAK [i] (17%) or combined FAK [i] and Src [i] (7%; Fig. 4 E). These data are consistent with cell proliferation defects observed at earlier time points (Fig. 4 D). In summary, these data demonstrate that cells treated with FAK [i] or Src [i] display defects in known functional readouts of these kinases (cell migration and proliferation) and confirm the inhibition of FAK and Src in cells treated with FAK [i] and Src [i].

FAK and Src inhibition reduce pY-dependent adhesion signaling without altering IAC protein composition

We have shown that IACs are robust to perturbation of the most connected kinase within the network, FAK, and that FAK and Src are inhibited effectively upon treatment with FAK [i] and Src [i], respectively. To investigate further the role of adhesome kinases upon the IAC network structure, IACs were isolated from cells treated with inhibitors and analyzed by immunoblotting to assess IAC composition and pY signaling events. Equal amounts of protein material were analyzed in each condition (Fig. 5 A), and the specificity of the IAC isolation was confirmed by detection of IAC proteins and the absence of non-IAC proteins (Tf receptor and BAK; Fig. 5 B). Kinase inhibition of FAK, Src, or FAK and Src combined did not affect the abundance of canonical IAC components, supporting the findings from MS upon FAK inhibition alone (Fig. 5, B and C). In contrast, immunoblotting of FAK and paxillin phosphorylation sites from isolated IACs demonstrated reduced levels of FAK^{Y397} (84%) and paxillin^{Y118} (73%) upon FAK and Src inhibition (Fig. 5, B and C), which was also observed in whole-cell extracts (Fig. 5, D and E). Immunoblotting against additional FAK- and Src-dependent phosphorylation sites demonstrated that FAK^{Y576} was most reduced upon combined FAK and Src inhibition, whereas p130Cas^{Y249} showed effects similar to those observed for paxillin^{Y118} (Fig. 5, D and E). These data demonstrate the specificity of FAK [i] and Src [i] and suggest that reduced phosphorylation levels of multiple IAC components do not elicit a major change in IAC composition.

To confirm that inhibition of FAK and/or Src activity altered IAC phosphorylation but not IAC composition, we performed a targeted analysis of selected IAC components and adhesion-dependent phosphorylation events and visualized their localization by immunofluorescence in cells treated with inhibitors (Fig. 6: pY and α5 integrin, A–C; FAK^{Y397} and vinculin, D–F; paxillin^{Y118} and paxillin, G–I). The cell area covered by pY-positive areas and the size and number of pY-positive areas was reduced upon FAK and Src inhibition individually and was almost completely depleted upon combined FAK and Src inhibition (Figs. 6, A and B; and Fig. S4 A). In addition, FAK^{Y397}- and paxillin^{Y118}-positive areas were reduced in cells treated with FAK [i] and Src [i] (Figs. 6, D, E, G, and H; and Fig. S4, C and E), respectively, which confirmed the abundance

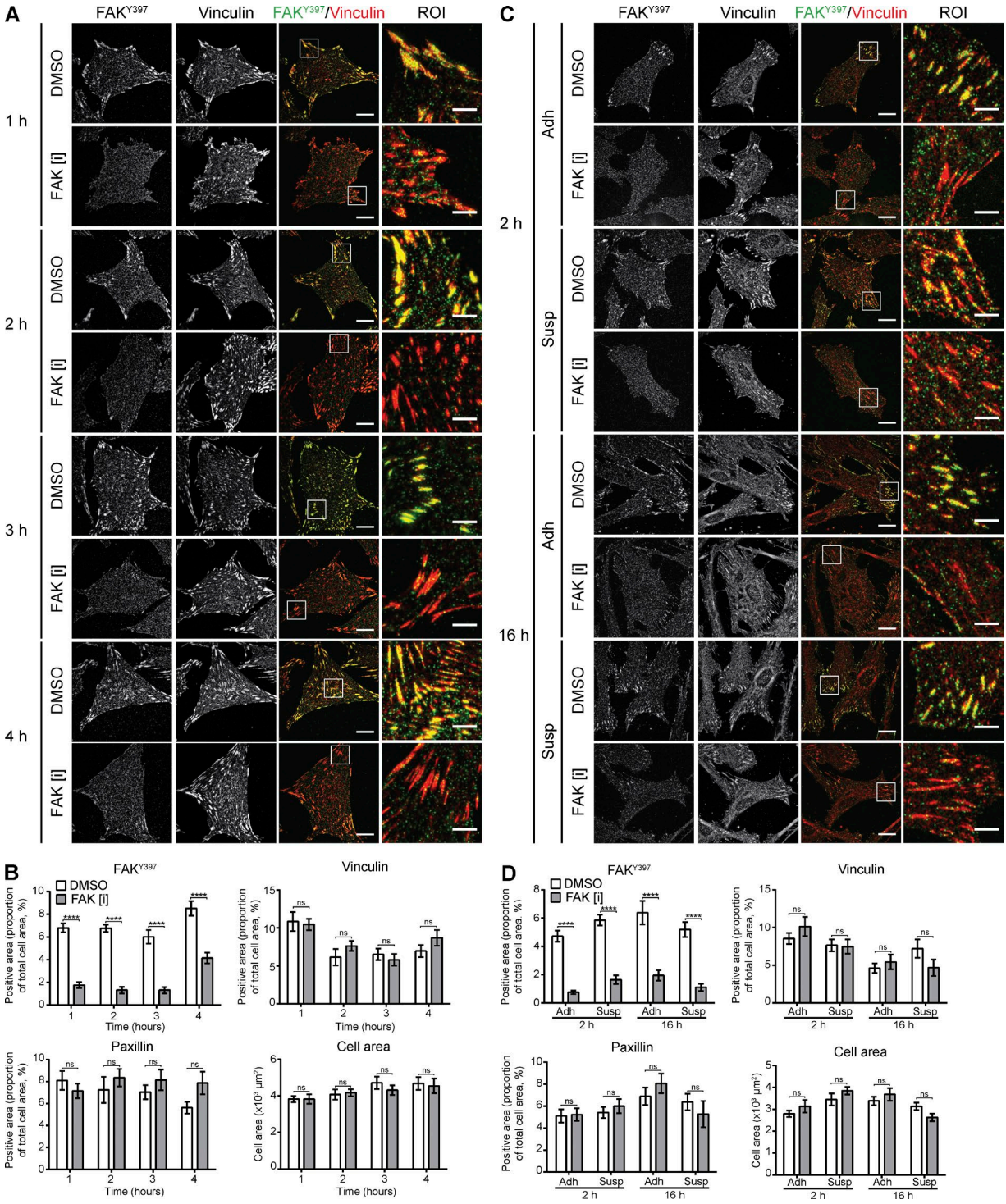

Figure 3. **Effects of the duration and timing of FAK inhibition on cell adhesion.** (A) Immunofluorescence staining of HFF cells spread on FN for 1 h and treated with DMSO or 3 µM FAK [i] for 1, 2, 3, or 4 h. IACs were visualized by staining for FAK^{Y397} (green) and vinculin (red). Bars: (main) 20 µm; (ROI) 5 µm. Additional images of paxillin-positive areas and the actin cytoskeleton are shown in Fig. S2 A. (B) Quantification of images in A and Fig. S2 A. Quantification of the cell area covered by FAK^{Y397}-, vinculin-, and paxillin-positive areas, and the total cell area (mean ± SEM; *n* = 10 cells, FAK^{Y397}, vinculin, and paxillin; *n* = 20 cells, cell area). (C) Immunofluorescence staining of HFF cells treated with FAK [i] added to suspension or prespread cells. To examine effects on cell spreading and IAC formation, DMSO or FAK [i] was added to HFF cells kept in suspension and cells were plated onto FN-coated plates (Susp). To examine effects on IAC maturation, cells kept in suspension were plated onto FN-coated plates for 1 h and treated with DMSO or FAK [i] (Adh). In both cases, cells were fixed after 2 or 16 h total spreading times. IACs were visualized by staining for FAK^{Y397} (green) and vinculin (red). Bars: (main) 20 µm; (ROI) 5 µm. Additional images of paxillin-positive areas and the actin cytoskeleton are shown in Fig. S2 B. (D) Quantification of images in C and Fig. S2 B. Quantification of the cell area covered by FAK^{Y397}-, vinculin- and paxillin-positive areas, and the total cell area (mean ± SEM; *n* = 20 cells, FAK^{Y397} and cell area; *n* = 10 cells, vinculin and paxillin). ****, P < 0.0001; ns, not significant; two-way analysis of variance with Tukey's post hoc correction (comparisons for each condition are shown). Representative images are shown.

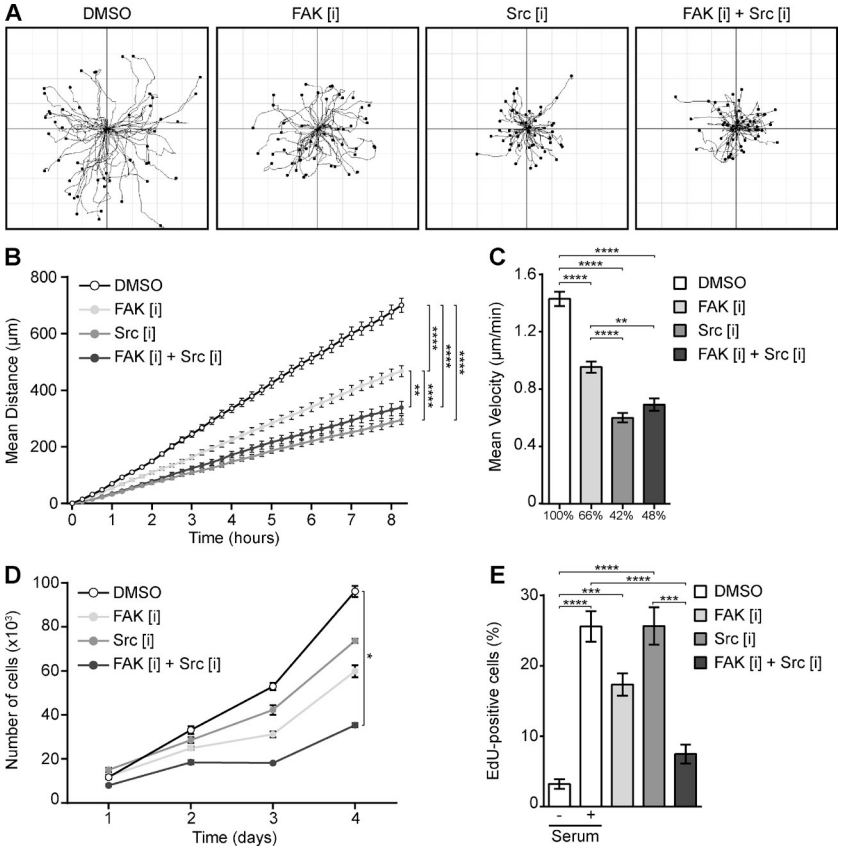

Figure 4. **Effects of FAK, Src and combined FAK and Src inhibition on cell migration and proliferation.** (A) Migration of HFF cells treated with DMSO, FAK [i], Src [i], or combined FAK [i] + Src [i] in scratch wound assays. Individual cells were tracked over 8 h. (B and C) Quantification of the distance (B) and velocity (C) of migrating cells in scratch wound assays. Percentage values relative to the DMSO condition are shown below bars (mean ± SEM, n = 50 cells per condition). In B, statistical significance was calculated based on the final time point. (D) Cells were incubated with DMSO or inhibitors for the required times, fixed and stained with 0.1% crystal violet. Additional inhibitors were added every 24 h, where appropriate, to maintain protein inhibition. Absorbance intensity was measured (590 nm) and a calibration curve was used to estimate total cell number in each condition (mean ± SEM, n = 3). Statistical significance was calculated using values from day 4. (E) Cells were incubated with DMSO or inhibitors for 16 h, EdU was added to cells 2 h before fixation, and the percentage of EdU-positive cells relative to DAPI staining in each field of view was calculated (mean ± SEM, n > 450 cells from 15 fields). Serum-starved cells were used as a negative control. *, P < 0.05; **, P < 0.01; ***, P < 0.001; ****, P < 0.0001, Kruskal–Wallis test with Dunn's post hoc correction.

changes of FAK^{Y397} and paxillin^{Y118} observed biochemically (Fig. 5). In contrast, the proportion of large (>1.5 µm^2) and small (<1.5 µm^2) IAC areas, and the number and size of IACs, was unchanged upon kinase inhibition for α5 integrin, vinculin, and paxillin (Fig. 6, C, F, and I; and Fig. S4, B, D, and F), indicating that the abundance of these IAC components was resistant to FAK and Src inhibition. These data also demonstrate that kinase inhibition did not result in the redistribution of these proteins to different types or size of IAC. Therefore, these data suggest that both the number and size of pY-positive areas are reduced upon kinase inhibition whereas protein levels of IAC components are unaffected. In summary, these data demonstrate further that IAC composition is largely unaffected, and robust to, FAK and Src inhibition, whereas phosphorylation of IAC proteins and thus adhesion signaling are affected by perturbation of FAK and/or Src catalytic activity.

FAK inhibition affects dynamics of SH2 domain-containing proteins in IACs

We have shown that disrupting FAK phosphorylation at FAK^{Y397} had little effect on the composition of IACs (Fig. 2 D and Table S2) but did result in altered adhesion signaling (Figs. 4, 5, and 6). To investigate how a lack of change in IAC composition could result in altered cell behavior upon FAK inhibition, we examined the dynamics of core IAC components (vinculin, paxillin, and FAK) and SH2 domain–containing proteins using a pY reporter (dSH2; Kirchner et al., 2003; Ballestrem et al., 2006) by FRAP in NIH3T3 cells (Fig. 7). Similarly to effects observed in HFFs, FAK inhibition with FAK [i] or PF228 resulted in a reduction of FAK^{Y397} levels but did not affect vinculin- or paxillin-containing IACs in these cells (Fig. S5). Upon FAK inhibition, there was no difference in the dynamics of vinculin or FAK in IACs and there was a small decrease in the half-time ($t_{1/2}$) of recovery for paxillin (Fig. 7, A–C). However, there was a larger decrease in the recovery half-time and a small increase in the mobile fraction (MF) for the dSH2 pY reporter upon FAK inhibition (Fig. 7, D–F), which indicates that pY-binding proteins displayed quicker dynamics and increased turnover upon FAK inhibition. These data suggest that changes in signaling (migration and proliferation) induced upon FAK inhibition and reduced phosphorylation events may be the result of altered dynamics of pY-binding proteins and lower-affinity binding of associated signaling components in IACs.

Discussion

To investigate the modularity of the IAC network and its sensitivity to pharmacological perturbation of key IAC signaling components, pharmacological inhibitors were used to perturb FAK and Src activities, and a combination of targeted and global approaches were used to analyze the effects of kinase inhibition on IAC composition and adhesion signaling. These analyses demonstrate that neither FAK nor Src activity is required to maintain IAC composition or regulate the proposed modular nature of IACs but is required for adhesion signaling and functions of these protein kinases, such as cell migration and proliferation. Furthermore, FRAP analysis demonstrated that pY-binding proteins displayed increased turnover upon FAK inhibition. These data indicate that altered dynamics of IAC proteins could be the mechanism by which IACs transduce signals while maintaining a stable structural connection to actin.

Inhibition of FAK and Src individually or in combination revealed different profiles of phosphorylation of IAC

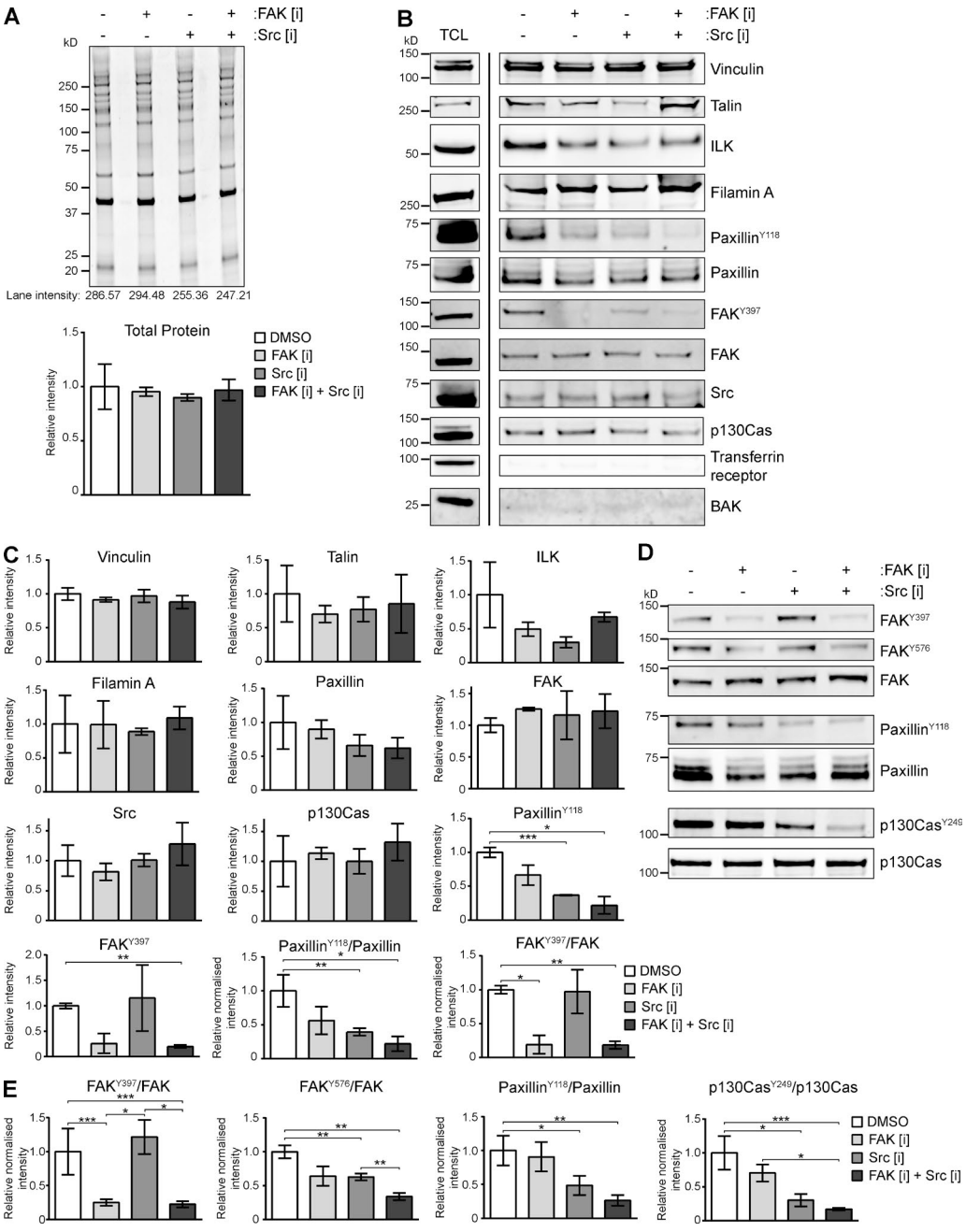

Figure 5. **Effects of FAK, Src, and combined FAK and Src inhibition on IAC composition.** (A and B) HFF cells spread on FN for 1 h were treated with DMSO, FAK [i], Src [i], or combined FAK [i] + Src [i] for 1 h. IACs were isolated using the workflow in Fig. 2 A and were analyzed by SDS-PAGE (A) and immunoblotting (B). Representative total protein intensity values for each lane are indicated. Graph shows intensity values normalized to the DMSO condition (mean ± SEM, $n = 3$). Cell lysates from cells spread on FN (TCL) were used as a positive control. Molecular mass values (kD) are displayed. (C) For quantification of immunoblotted membranes in B, the band intensity values for each protein are shown relative to the DMSO condition (mean ± SEM, $n = 3$). Quantification was not performed for Tf receptor or BAK. (D) Total cell lysates collected from HFF cells spread on FN for 1 h and treated with DMSO or inhibitors for 1 h were analyzed by immunoblotting. Molecular mass values (kD) are displayed. (E) For quantification of immunoblotted membranes in D, phosphorylation values normalized to the corresponding total protein values are shown relative to the DMSO condition (mean ± SEM; $n = 4$, FAK^{Y397}, FAK^{Y576}, and paxillin^{Y118}; $n = 3$, p130Cas^{Y249}). *t* test: *, $P < 0.05$; **, $P < 0.01$; ***, $P < 0.001$. Representative images are shown.

proteins. Similar to studies treating cells with other FAK inhibitors (Slack-Davis et al., 2007; Tanjoni et al., 2010; Stokes et al., 2011), FAK [i] did not completely abolish FAK^{Y397} levels, which indicates that other kinases are able to phosphorylate this phosphosite. FAK autophosphorylation at FAK^{Y397} has been shown to occur through FAK dimerization (Brami-Cherrier et al., 2014), and inhibitors blocking FAK dimerization may be required to inhibit FAK activation entirely. FAK [i] inhibited FAK^{Y397} to a greater extent than Src [i], and in agreement with studies showing that a reduction in FAK^{Y397} does not affect p130Cas phosphorylation (Tanjoni et al., 2010), Src [i] inhibited the Src substrates paxillin^{Y118} and p130Cas^{Y249} to a greater extent than FAK [i], which suggests that FAK [i] and Src [i] specifically inhibit FAK and Src, respectively. The inability of FAK [i] to cause a substantial reduction of Src substrates suggests that a substantial decrease in FAK^{Y397} alone does not abolish

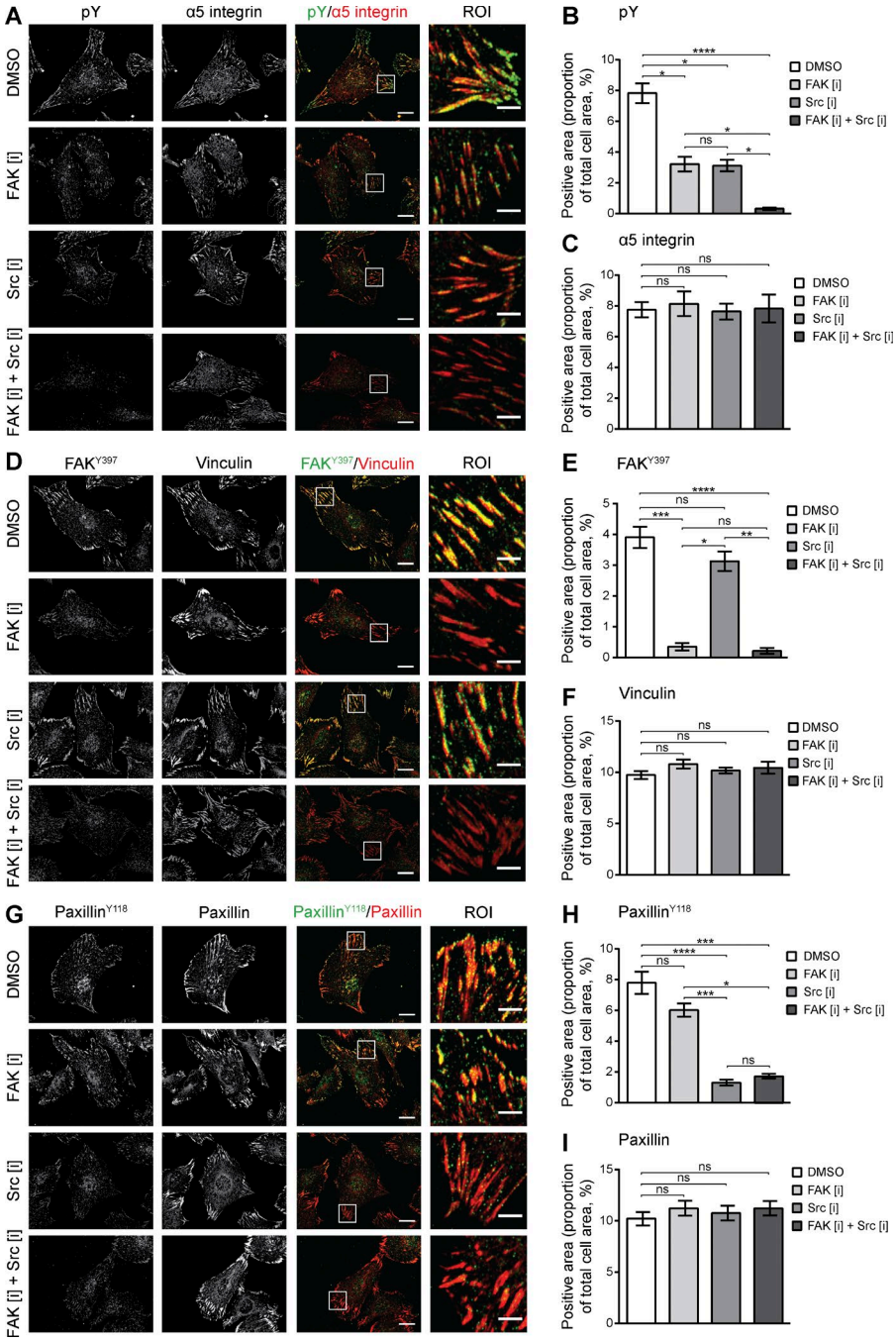

Figure 6. **Effects of FAK, Src and combined FAK and Src inhibition on IAC proteins and phosphorylation.** (A–I) HFF cells spread on FN for 1 h were treated with DMSO, FAK [i], Src [i], or combined FAK [i] + Src [i] for 1 h. IACs were visualized by staining for pY (green) and α5 integrin (red; A–C), FAK^{Y397} (green) and vinculin (red; D–F) or paxillin^{Y118} (green) and paxillin (red; G–I). Bars: (main) 20 µm; (ROI) 5 µm. Graphs show quantification of the cell area covered by positive staining of the indicated protein (mean ± SEM, n = 10 cells). *, P < 0.05; **, P < 0.01; ***, P < 0.001; ****, P < 0.0001; ns, not significant; Kruskal–Wallis test with Dunn's post hoc correction (in C, F, and I, comparisons with cells treated with DMSO are shown). Representative images are shown.

Src activity, possibly because Src has already been activated by FAK, high enough levels of FAK^{Y576} are maintained to enable additional Src activation, or Src activation occurs through alternative FAK-independent mechanisms. Src inhibition resulted in a decrease in FAK^{Y576}, paxillin^{Y118}, and p130Cas^{Y249}; however, these phosphosites and total pY were all further reduced upon combined FAK and Src inhibition that also reduced FAK^{Y397} (Fig. 5). In addition, it is surprising that adhesion signaling via pY was almost completely abolished upon inhibition of only two IAC kinases because several kinases have been reported to localize to IACs and modify their components (Winograd-Katz et al., 2014; Robertson et al., 2015). Therefore, these data suggest that FAK and Src are the key adhesome kinases that regulate adhesion signaling via pY, which places importance on their regulators to control activation state.

Previous studies have shown that FAK-null cells, cells overexpressing the FAK-related nonkinase (FRNK, a dominant-negative portion of FAK that inhibits phosphorylation at FAK^{Y397}; Richardson and Parsons, 1996) and cells treated with the Src inhibitor PP2 display defects in cell migration (Ilić et al., 1995; Sieg et al., 1999; Slack et al., 2001). Similarly, FAK and Src have been shown to regulate cell proliferation in several cell types (Gilmore and Romer, 1996; Sánchez-Bailón et al., 2012; Serrels et al., 2012; Luo et al., 2013; Je et al., 2014). In agreement with these data, we found that perturbation of FAK and/or Src kinase activity resulted in defects in cell migration and proliferation, which was particularly apparent when both kinases were inhibited. However, previously reported defects during early cell spreading upon FAK inhibition and cell attachment upon FRNK overexpression (Richardson and Parsons, 1996)

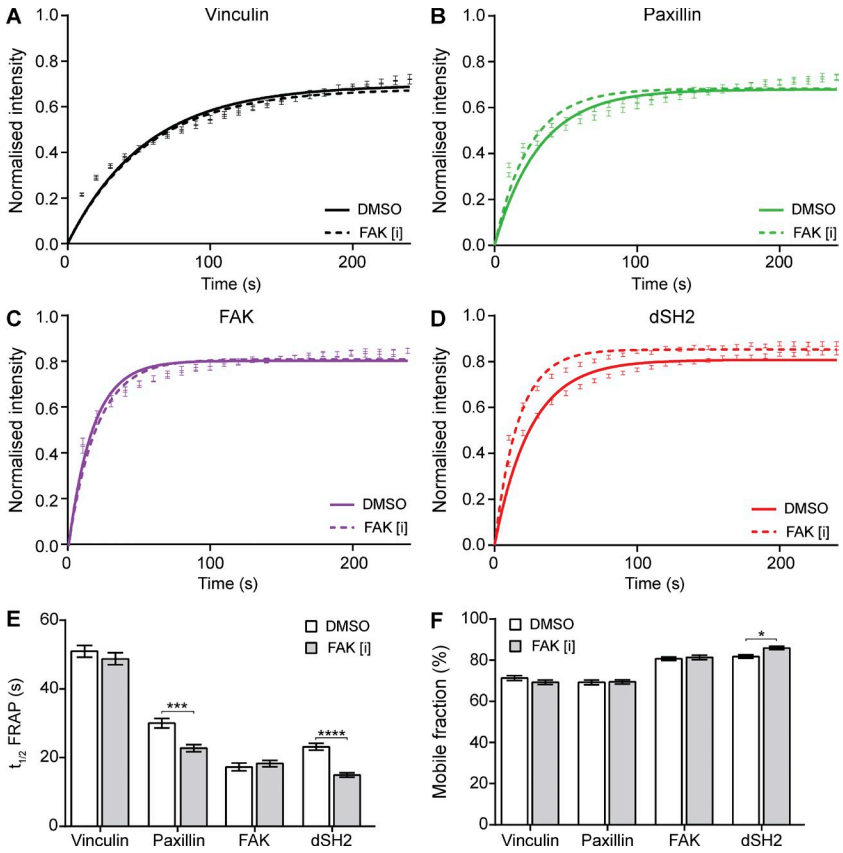

Figure 7. **FAK inhibition modifies the turnover rate of paxillin and SH2 domain proteins.** (A–D) FRAP curves for IACs in NIH3T3 fibroblasts transfected with the indicated GFP- or YFP-tagged IAC protein. Cells were treated with DMSO or 3 µM FAK [i] for 1 h before imaging. (E and F) Graphs show half-time (E) and MF (F) values for each IAC protein, calculated from the above FRAP curves (mean ± SEM; five IACs per cell, six to eight cells analyzed per experiment). *, P < 0.05; ***, P < 0.001; ****, P < 0.0001; one-way ANOVA with Sidak's post hoc test. Data shown are pooled from four independent experiments.

were not observed here. This may be because cells were able to overcome those effects at the later time points investigated here, or because it is the scaffolding role of FAK that mediates cell spreading, supported by data showing that coexpression of Src or catalytically inactive FAK can rescue cell spreading defects (Richardson et al., 1997) and endogenous FRNK expression is increased during the early stages of cell attachment (Nagoshi et al., 2006), indicating that FAK catalytic activity does not regulate this process. However, we found that pY-binding proteins displayed increased dynamics in IACs upon FAK inhibition, indicating that altered adhesion signaling may be the result of altered dynamics of IAC components rather than changes to IAC composition. It has recently been reported that IAC components display altered dynamics that occur independently to changes in IAC composition when cells are exposed to different stiffnesses in 3D environments (Doyle et al., 2015), which provides further evidence that changes to the dynamics of IAC components may be critical for signal transduction.

It has been reported that IACs increase in size upon FAK inhibition, although the proportion of small versus large IACs was unaffected (Plotnikov et al., 2012). Conversely, FAK inhibition was shown to result in the loss of paxillin-containing IACs (Slack-Davis et al., 2007). Many studies have reported changes in the morphology or number of IACs in FAK-null cells (Ilić et al., 1995; Sieg et al., 1999; Ren et al., 2000; Schober et al., 2007; Dumbauld et al., 2010). It has also been reported that IAC turnover is slower upon FRNK overexpression (Ezratty et al., 2005), upon overexpression of FAK that cannot be phosphorylated by Src (Westhoff et al., 2004), upon FAK depletion (Chan et al., 2010), or prevention of FAK phosphorylation at FAK^{Y397} (Webb et al., 2004). However, this raises an important issue regarding the signaling and scaffolding roles of FAK, because studies have shown effects of FAK knockdown that are not always recapitulated upon inhibition of FAK kinase activity. For example, it has been shown that IACs increase in size upon mechanical stimulation in control cells and in cells expressing a FAK mutant that cannot be phosphorylated at FAK^{Y397}, but this effect was not observed in FAK-null cells (Wang et al., 2001), and that FAK expression but not kinase activity is required for cell motility in response to platelet-derived growth factor and epidermal growth factor (Sieg et al., 2000). In addition, it has been reported that the FAK-related kinase Pyk2 and Src are able to compensate for the loss of FAK (Sieg et al., 1998), indicating that the genetic background of FAK-null cells is altered. Here, we inhibited FAK using small-molecule inhibitors over a relatively short time frame to minimize these effects and examined the effects of reducing pY levels in preformed, steady-state IACs while maintaining the scaffolding role of FAK.

IACs have been shown to vary in size in response to inhibitors that affect the cytoskeletal networks, such as inhibitors targeting microtubule polymerization (Bershadsky et al., 1996; Ezratty et al., 2005; Ng et al., 2014; Yue et al., 2014), myosin-II activity (Choi et al., 2008; Pasapera et al., 2010; Schiller et al., 2011, 2013; Kuo et al., 2012; Horton et al., 2015a), Rho-mediated contractility (Chrzanowska-Wodnicka and Burridge, 1996; Imamura et al., 2000), and, more recently, cyclin-dependent kinase 1 (Robertson et al., 2015). In contrast, IACs are robust to gene knockouts of IAC proteins in silico (Zaidel-Bar et al., 2007) and to prevention of FAK localization to IACs in vitro (Gilmore and Romer, 1996). In combination with findings from these studies, the data presented here support a model whereby IACs are robust cellular structures whose complex network of interactions maintains their composition upon modulation of individual components and adhesion signaling, but IACs are

affected by modulation of external factors such as force or microtubule targeting. Small changes in IAC composition upon FAK inhibition, particularly concerning transiently associating IAC proteins, may be important biologically and are not detected here because of the sensitivity of the proteomic approach. Alternatively, reducing pY levels in IACs, which consequently disrupts the binding of tyrosine-phosphorylated proteins and SH2 domain-containing proteins, may not cause a dramatic change in the composition of IACs because of the highly connected and complex nature of the IAC network that compensates for the loss of this particular protein–protein interaction. In addition, it is possible that IACs still contain some pY upon FAK inhibition, which consequently would not result in the complete dissociation of pY-binding proteins from IACs.

In summary, the data presented here suggest that kinase-dependent signal flux can propagate through IACs without causing gross changes to IAC composition, which suggests that separation in IAC protein composition and pY-dependent signaling is possible at IACs. This raises the question of how IACs relay chemical signals while maintaining a mechanical connection between integrins and actin, which may occur through altered dynamics of associated signaling components in IACs.

Materials and methods

Cell culture

Telomerase-immortalized HFF cells (provided by K. Clark, University of Leicester, Leicester, England, UK) and mouse embryo fibroblast (NIH3T3) cells were maintained in DMEM supplemented with 10% (vol/vol) FCS (Lonza Bioscience) and 2 mM L-glutamine, penicillin, and streptomycin and incubated at 37°C in a humidified 5% (vol/vol) CO_2 atmosphere.

Reagents and antibodies

Bovine plasma FN, human Tf, PBS containing $CaCl_2$ and $MgCl_2$ (PBS+), $CaCl_2$- and $MgCl_2$-free PBS (PBS−), DMEM, and DMEM containing 25 mM Hepes (DMEM-Hepes) were purchased from Sigma-Aldrich. Monoclonal antibodies used were rat anti-α5 integrin (mAb11; IF, 1:200; gift from K. Yamada, National Institutes of Health, Bethesda, MD), mouse anti-FAK (clone 77; IB, 1:1,000; 610088; BD Biosciences), rabbit anti-FAK^{Y397} (clone 141–9; IB, 1:500; IF, 1:200; 44-625G; Invitrogen), rabbit anti-ILK (EPR1592; IB, 1:1,000; ab76468; Abcam), mouse anti-p130Cas (clone 21; IB, 1:1,000; 610272; BD Biosciences), mouse anti-p130Cas^{Y249} (clone J169-757.12.2; IB, 1:1,000; 558401; BD Biosciences), mouse anti-paxillin (clone 349; IB, 1:1,000; IF, 1:400; 610051; BD Biosciences), mouse anti-pY (P-Tyr-100; IF, 1:400; 9411; Cell Signaling Technology), mouse anti–Tf receptor (H68.4; IB, 1:1,000; 13–6890; Invitrogen), and mouse anti-vinculin (hVIN-1; IB, 1:1,000; IF, 1:400; V9131; Sigma-Aldrich). Polyclonal antibodies used were rabbit anti-BAK (IB, 1:1,000; B5897; Sigma-Aldrich), rabbit anti-FAK^{Y576} (IB, 1:500; 44-652G; Invitrogen), rabbit anti–filamin A (IB, 1:1,000; A301-135A; Bethyl Laboratories), rabbit anti-paxillin^{Y118} (IB, 1:500; IF, 1:200; 44-722G; Invitrogen), rabbit anti-Src (IB, 1:1,000; 2108BC; Cell Signaling Technology), rabbit anti-Src^{Y416} (IB, 1:500; 2101BC; Cell Signaling Technology), and goat anti-talin (clone c-20; IB, 1:1,000; sc-7534; Santa Cruz Biotechnology). Secondary Alexa Fluor 680–conjugated (1:5,000; Invitrogen) or Alexa Fluor 800–conjugated (1:5,000; Invitrogen) anti–mouse, –rabbit or –goat antibodies were used for immunoblotting. For immunofluorescence, secondary Alexa Fluor 488–conjugated (1:200; Invitrogen) and Alexa Fluor 594–conjugated (1:200; Invitrogen) anti–rabbit, –rat, or –mouse antibodies were used. Actin filaments were visualized by Alexa Fluor 647–conjugated phalloidin (1:200; Invitrogen). The FAK-specific inhibitor AZ13256675 (FAK [i]) and Src-specific inhibitor AZD0530 (Src [i]) were obtained from Astra Zeneca and are available from the pharmacology toolbox (http://openinnovation.astrazeneca.com/what-we-offer/pharmacology-toolbox/). PF271 and PF228 were obtained from Sigma-Aldrich.

Recombinant and cell-based kinase assays

To examine the potency of FAK [i], the IC_{50} values for FAK [i] and PF271 against FAK^{Y397} were calculated in a recombinant kinase assay and cell-based assay. For the cell-based assay, adherent HEK293 cells were transiently transfected with a plasmid coding for 3′ cMyc-tagged, full-length FAK (pcDNA3.2 FAK_cMyc; Astra Zeneca) using Lipofectamine 2000. Cells were detached and resuspended in DMEM-Hepes supplemented with 1% (vol/vol) FCS. Transfected cells were seeded at 1.25×10^5 cells/ml, allowed to adhere overnight, and incubated with FAK [i] or PF271 for 90 min. Cells were lysed, and lysates were transferred to ELISA 384-well plates (Greiner) precoated with a mouse anti-cMyc monoclonal antibody (9B11; cs2276; Cell Signaling Technology). Subsequently, plates were washed with PBS− and incubated with a rabbit anti-FAK^{Y397} polyclonal antibody (44-624G; Invitrogen). Plates were washed again before addition of an anti–rabbit HRP-conjugated secondary antibody (cs7074; Cell Signaling Technology). After incubation at RT, plates were washed with PBS− and QuantaBlu fluorogenic peroxidase substrate solution (15169; Thermo Fisher Scientific) was added to each well. Plates were read using a plate reader (Tecan Ultra or Tecan Safire).

To examine the selectivity of FAK [i], both FAK [i] and PF271 were screened against a panel of recombinant enzymes using a similar approach that has been described previously (Davies et al., 2000; Bain et al., 2003). In addition, IC_{50} values were calculated for FAK. Table S1 lists the enzymes tested and the percentage inhibition remaining after incubation with 1 µM of either inhibitor relative to control.

Plating cells

Cells were washed with PBS− and detached with trypsin (Sigma-Aldrich), and trypsin was quenched with 2.5% (wt/vol) BSA in DMEM-Hepes. Cells were washed in PBS− and resuspended in 5% (wt/vol) BSA in DMEM-Hepes and incubated at 37°C in a humidified 8% (vol/vol) CO_2 atmosphere in suspension for 30 min to downregulate adhesion-dependent signaling events. Cells were washed in PBS−, and 1.5×10^6 cells were plated in DMEM-Hepes on 10-cm-diameter dishes (Corning) coated with FN (10 µg/ml, PBS+) or Tf (50 µg/ml, PBS−). Before ligand coating, dishes were blocked with heat-denatured BSA (10 mg/ml of >99% purity BSA, 0.22 µm filtered, 85°C for 12 min) at RT for 1 h. Cells were incubated at 37°C in a humidified 8% (vol/vol) CO_2 atmosphere for the required times.

Collection of cell lysates

For collection of cell lysates, cells were seeded at 3×10^5 cells/ml for 1 h and DMSO or inhibitors were added at the required concentration. Inhibitors were added from stock solutions to give a final dilution of 1:1,000 except for combined FAK [i] and Src [i] treatment, where the final dilution from stock solutions was 1:2,000 for each inhibitor. In the case that cells were plated in the presence of inhibitors, inhibitors or DMSO were added to cells when maintained in suspension and cells were plated directly from suspension. Medium from dishes was removed, and dishes were washed once in cold PBS−. Lysates of adherent cells were collected by scraping in lysis buffer (1% [vol/vol] Triton X-100, 150 mM NaCl, 10 mM $MgCl_2$, 5 mM EDTA, 10 µg/ml leupeptin, 10 µg/ml aprotinin, 0.5 mM 4-(2-aminoethyl)benzenesulfonyl

fluoride hydrochloride, and 10 mM Na_3VO_4, pH 7.4). For collection of suspension cells, cells in suspension were centrifuged (450 *g*, 4 min, 4°C) and washed in cold PBS- before addition of lysis buffer. After cell lysis, nonsolubilized material was discarded by centrifugation (22,000 *g*, 10 min, 4°C). To ensure equal total protein gel loading, relative protein amounts in each sample were calculated using a BCA protein assay kit (23225; Thermo Fisher Scientific).

IAC isolation

IACs were isolated using a similar approach to the ligand affinity purification method described previously (Jones et al., 2015). Cells were spread on FN or Tf for 1 h, treated with inhibitors or DMSO for 1 h, and incubated with dimethyl-3, 3′-dithiobispropionimidate (DTBP; 6 mM, 5 min; Thermo Fisher Scientific). DTBP was removed and quenched with 200 mM Tris-HCl, pH 8 (3 min), cells were washed in cold PBS−, and cell bodies were removed by incubation in cold RIPA buffer (50 mM Tris-HCl, pH 8.0, 1% [vol/vol] Triton X-100, 150 mM NaCl, 5 mM EDTA, 0.5% [wt/vol] SDS, and 1% [wt/vol] sodium deoxycholate, 3 min) followed by a high-pressure water wash. Protein complexes were washed and stored in cold PBS−. Protein complexes were collected by scraping in 30-µl/dish adhesion recovery solution (125 mM Tris-HCl, pH 6.8, 1% [wt/vol] SDS, and 15% [vol/vol] β-mercaptoethanol) and heated to 95°C for 10 min. Four times sample volume of −20°C acetone was added to samples, and samples were incubated at −80°C for at least 3 h. Samples were washed three times with acetone (16,000 *g*, 15 min, 4°C), and samples were allowed to dry (37°C for 20–30 min). Precipitated complexes were resuspended in 2× reducing sample buffer (50 mM Tris-HCl, pH 6.8, 10% [vol/vol] glycerol, 4% [wt/vol] SDS, 0.004% [wt/vol] bromophenol blue, and 15% [vol/vol] β-mercaptoethanol) and heated to 70°C for 20 min.

SDS-PAGE and immunoblotting

Protein samples were separated by SDS-PAGE (4–12% [wt/vol] NuPAGE Novex Bis-Tris gels; Invitrogen) at 200 V for 45 min. To visualize total protein, gels were incubated in Instant Blue (Expedeon) for 1 h and washed in water overnight at 4°C. For immunoblotting, gels were transferred onto nitrocellulose membrane (Whatman) and membranes were blocked with blocking buffer (Sigma-Aldrich) in PBS− for 1 h at RT. Membranes were incubated with appropriate concentrations of primary antibodies diluted in blocking buffer in TBS (10 mM Tris-HCl, pH 8.0, and 100 mM NaCl) supplemented with 0.05% (vol/vol) Tween-20 (TBS-T) overnight at 4°C. After three washes with TBS-T, membranes were incubated with appropriate secondary antibodies diluted in blocking buffer in TBS-T for 45 min at RT in the dark and were washed three times in TBS-T. Secondary antibodies used were donkey Alexa Fluor 680–conjugated anti–goat IgG, anti–mouse IgG, or anti–rabbit IgG (Life Technologies) and donkey IRDye 800–conjugated anti–mouse IgG (Rockland Immunochemicals). Membranes and stained gels were scanned using the Odyssey infrared imaging system (LI-COR), and total lane intensities were determined using Odyssey software (LI-COR).

In-gel digestion and peptide desalting

Protein samples were separated by SDS-PAGE at 200 V for 2 min or until all samples had migrated into the gel. The gel was stained with Instant Blue (Expedeon), and gel lanes were cut into 1-mm^3 pieces and washed twice with 50% (vol/vol) acetonitrile (ACN) in 12.5 mM NH_4HCO_3 and twice with ACN to dry gel pieces. Proteins were reduced by incubation in 10 mM DTT diluted in 25 mM NH_4HCO_3 for 1 h at 56°C and alkylated in 55 mM iodoacetamide diluted in 25 mM NH_4HCO_3 for 45 min at RT in the dark. Gel pieces were washed with 25 mM NH_4HCO_3 followed by a wash in ACN, which was repeated once more. Gel pieces were dried and incubated with 12 µg/ml trypsin overnight at 37°C to enable complete protein digestion (Shevchenko et al., 1996). Digested peptides were extracted by incubation with ACN in 0.2% (vol/vol) formic acid (FA) followed by incubation with 50% (vol/vol) ACN in 0.1% (vol/vol) FA. To desalt peptides, each sample was resuspended in 5% (vol/vol) ACN in 0.1% (vol/vol) FA followed by incubation with OLIGO R3 beads (Applied Biosystems). Bead-bound peptides were washed twice in 0.1% (vol/vol) FA, eluted by two washes in 50% (vol/vol) ACN in 0.1% (vol/vol) FA, dried, and resuspended in 5% (vol/vol) ACN in 0.1% (vol/vol) FA.

Liquid chromatography tandem MS data acquisition and analysis

Peptides were analyzed by liquid chromatography tandem MS using an UltiMate 3000 Rapid Separation LC (Dionex) coupled to an Orbitrap Elite mass spectrometer (Thermo Fisher Scientific). Peptide samples were loaded onto a precolumn (20 mm × 180 µm i.d.; Waters) in biological sample order rather than biological replicate order to increase likelihood of chromatograph alignment between samples in downstream analyses (D. H. J. Ng, unpublished data). Peptides were separated on an analytical column (250 mm × 75 µm i.d., 1.7 µm particle size, bridged ethyl hybrid C_{18}; Waters) over a 2-h gradient from 8 to 33% (vol/vol) ACN in 0.1% (vol/vol) FA at a flow rate of 200 nl/min. Liquid chromatography tandem MS analyses were performed in data-dependent mode to allow automatic selection of peptides for fragmentation.

Raw files were analyzed and preprocessed using Progenesis software (Progenesis QI, Nonlinear Dynamics; http://www.nonlinear.com/progenesis/qi-for-proteomics/) with automatic detection of alignment reference, which was selected as FAK [i], biological replicate 2 (R2). MS data were searched using an in-house Mascot server (version 2.2.03; Matrix Science; Perkins et al., 1999) against the UniProt_Human protein sequence database. Permitted fixed and variable modifications were cysteine carbamidomethylation and methionine oxidation, respectively. Only tryptic peptides with a maximum of one missed cleavage were considered. Only doubly or triply charged monoisotopic precursor ions were considered, peptide mass tolerance was set to ±5 p.p.m, and MS/MS tolerance was set to ±0.5 D.

Protein identifications were imported into Progenesis software and relative quantification was performed using protein grouping with nonconflicting (unique) peptides. Data were exported as protein measurements, and duplicate protein entries by gene name annotation were combined by addition of raw intensity values of unique peptides. Raw abundance values were normalized to the total raw abundance value in each condition. The dataset was filtered to include only proteins containing a minimum of two unique peptides that were used for protein quantification (Table S2). Log_2 fold change values for each of three biological replicates were calculated between DMSO and FAK [i] conditions using normalized raw values and the mean taken. In the case that a protein was not identified in all biological replicates, the mean fold change was based on the other biological replicate values only. P values were calculated from normalized abundance values between DMSO and FAK [i] conditions using the Holm–Sidak method for multiple comparisons (Holm, 1979). Each protein was analyzed individually, without assuming a consistent standard deviation. Alternatively, raw abundance values were normalized to the raw abundance value for vinculin (Table S3). MS data were deposited in ProteomeXchange (proteomecentral.proteomexchange.org) via the PRIDE partner repository (Vizcaíno et al., 2013) with the dataset identifier PXD002720 (DOI: 10.6019/PXD002720).

A list of SH2 domain-containing proteins was extracted from InterPro (Mitchell et al., 2015). Protein–protein interaction network analysis was performed using Cytoscape (version 3.02; Cline et al., 2007). Proteins identified by MS were mapped onto a merged human interactome (provided by A. Byron, University of Edinburgh, Edinburgh,

Scotland, UK) consisting of protein–protein interactions reported in the Protein Interaction Network Analysis platform (release date December 10, 2012; Wu et al., 2009), the MatrixDB database (release date April 20, 2012; Chautard et al., 2009) and the literature-curated integrin adhesome (Zaidel-Bar et al., 2007; Winograd-Katz et al., 2014). FAK, β1 integrin and their associated interacting proteins were extracted and displayed as a network (Fig. S1 D).

Immunofluorescence microscopy

Cells were plated on poly-D-lysine–coated glass-bottom dishes (14 mm diameter; MatTek) or ethanol-washed coverslips (13 mm diameter; VWR International) coated with FN (10 µg/ml). After appropriate inhibitor or DMSO incubation, cells were washed in PBS−, fixed in 4% (wt/vol) paraformaldehyde for 7 min at RT, washed in PBS−, and permeabilized with 0.5% (vol/vol) Triton X-100 for 10 min at RT. Permeabilized cells were washed three times with PBS− before incubation with appropriate primary antibodies diluted in 2% (wt/vol) BSA in PBS− for 1 h at RT. Cells were washed three times with PBS− and incubated with appropriate secondary antibodies diluted in 2% (wt/vol) BSA in PBS− for 30 min at RT in the dark. Stained cells were washed once in PBS−, twice in water and stored in water at 4°C until imaging. Alternatively, cells on coverslips were mounted onto glass slides (Klinipath) in polyvinyl alcohol mounting medium (Sigma-Aldrich).

Images of cells plated on glass-bottom dishes were acquired on a Delta Vision (Applied Precision) microscope using a 60×/1.42 Plan Apo objective and the Sedat filter set (86000v2; Chroma) at RT. Images were collected with a *Z* optical spacing of 0.2 µm using a Coolsnap HQ camera (Photometrics) and Softworx software (Applied Precision). Alternatively, images of cells plated on glass coverslips were acquired on a BX51 upright microscope (Olympus) using a 60×/1.25 Plan Fln objective and specific band pass filter sets. Images were captured using a Coolsnap EZ camera (Photometrics) and MetaVue software (Molecular Devices). Exposure times for each channel were maintained when imaging cells treated with different inhibitors.

Image analysis

Single slices of raw images were background filtered (rolling ball, 20-pixel radius) using ImageJ (version 1.48o; National Institutes of Health; Schindelin et al., 2012). Areas containing positive staining of IAC proteins (≥10 pixels) were measured and normalized to total cell area. In addition, the number and size of positive areas per cell was calculated.

FRAP

NIH3T3 fibroblasts were transfected with the required GFP- or YFP-tagged DNA constructs (vinculin-GFP, paxillin-GFP, FAK-GFP, or dSH2-YFP) and incubated overnight at 37°C. Before imaging, the supplemented medium was replaced with 2 ml Ham's F12 medium (Sigma-Aldrich) supplemented with 25 mM Hepes, 1% (vol/vol) L-glutamine, 1% (wt/vol) penicillin/streptomycin, and 2% (vol/vol) FCS, adjusted to pH 7.3. At this point, 3 µM FAK [i] or an equivalent volume of DMSO was also added to the medium. Cells were placed in the microscope chamber at 37°C for 1 h.

Cells were imaged using a CSU-X1 spinning disc confocal (Yokagowa) on a Axio-Observer Z1 microscope (Carl Zeiss) with a 60×/1.40 oil Plan-Apochromat objective, Evolve EMCCD camera (Photometrics), and motorized XYZ stage (ASI). The 488-nm laser was controlled using an Acousto-optical tunable filter through the laserstack (Intelligent Imaging Innovations [3i]). Three images were taken before photobleaching, and five IACs were bleached per cell with the 488-nm laser. Slidebook software was used to capture images every 10 s for a period of 4 min after photobleaching. Movies were analyzed using Slidebook software and MATLAB, with a script developed in-house as described previously (Humphries et al., 2007). In brief, corrected recovery fluorescence intensities were normalized to intensity before bleaching. The MF was calculated using the formula $MF = 100 \times (F_{infl} - F(0))/(F_{pre} - F(0))$, where F_{pre} is the prebleach intensity of bleached area, F_{inf} is the maximal postbleach intensity, and F(0) is the postbleach intensity at time 0 in the bleached area. For determination of recovery half-time ($t_{1/2}$), the normalized recovery data were fitted to the single exponential equation $F(t) = MF \times (1 - e^{\tau t})$ and the $t_{1/2}$ was calculated by $t_{1/2} = \ln 0.5/-\tau$.

Migration assay

For scratch wound migration assays, 2×10^6 cells were seeded into six-well plates in DMEM supplemented with 10% (vol/vol) FCS and 2 mM L-glutamine. After overnight incubation at 37°C in a humidified 5% (vol/vol) CO_2 atmosphere, pipette tips were used to wound cell monolayers. Cells were washed in DMEM to remove detached cells, and inhibitors or DMSO was added at the required dose. Cells were maintained at 37°C in a humidified 5% (vol/vol) CO_2 atmosphere and point visiting was used to allow imaging at multiple positions within the same time course. Bright-field images were acquired every 5 min over 8 h and 15 min on an AS MDW live-cell imaging system (Leica Microsystems) using a 20×/0.5 HC Plan Fluotar objective, a Coolsnap HQ CCD camera (Photometrics), and Image Pro software (version 6.3; Media Cybernetics). Cell migration was tracked manually using the ImageJ plugin MTrackJ (Meijering et al., 2012) for five cells per scratch wound. Quantification was performed using the Chemotaxis and Migration Tool (version 1.01; ibidi) in ImageJ (Schindelin et al., 2012).

Proliferation assays

To measure total cell number, a crystal violet staining assay was used. Initially, 2×10^4 cells were seeded into 12-well plates in DMEM supplemented with 10% (vol/vol) FCS and 2 mM L-glutamine. After 1-h incubation at 37°C in a humidified 8% (vol/vol) CO_2 atmosphere, the required concentration of inhibitors and DMSO were added to each well and cells were incubated at 37°C in a humidified 5% (vol/vol) CO_2 atmosphere for up to 4 d. Where applicable, additional inhibitors and DMSO were added every 24 h to maintain kinase inhibition. At required times, cells were washed in PBS−, fixed in 4% (wt/vol) paraformaldehyde for 15 min and stored in water at 4°C. Once all samples were collected, cells were stained with a 0.1% (wt/vol) crystal violet solution for 20 min and washed three times in water to remove excess stain. Samples were dried and stained cells were extracted in 2 ml/well 10% (vol/vol) acetic acid for 20 min. In duplicate, 200 µl crystal violet–stained cells were loaded into a 96-well plate, absorbance was read with a spectrometer at 590 nm, and the mean was taken to give a final absorbance value for each condition for that biological replicate (for each condition, $n = 2$ technical replicates and $n = 3$ biological replicates). Additionally, serial dilutions of a known number of cells were spread for 2 h and stained, and the absorbance was measured to give a calibration curve of absorbance versus total cell number ($y = 0.0014x + 0.0185$, $R^2 = 0.9821$; y, absorbance intensity; x, cell number [$\times 10^3$]), which was used to infer total cell number in the DMSO- and inhibitor-treated conditions.

To calculate the proportion of actively dividing cells, the Click-iT EdU Alexa Fluor 488 Imaging kit (Thermo Fisher Scientific) was used according to manufacturer's instructions. In brief, cells were plated in DMEM supplemented with 10% (vol/vol) FCS and 2 mM L-glutamine for 1 h and incubated with DMSO, FAK [i], Src [i], or combined FAK [i] and Src [i] for 16 h, and EdU was added to the medium 2 h before fixation. Serum-starved cells were used as a negative control. Stained cells were imaged and counted, and the percentage of EdU-positive cells relative to the total number of cells was calculated for each field of view. For each condition, at least 450 cells were counted from 15 fields of view.

Statistical analyses

Statistical significance was calculated as indicated in the figure legends with $P < 0.05$ considered statistically significant. All graphs and statistical analyses were performed using Prism (version 6.04; GraphPad). Figures were assembled using Illustrator (Adobe).

Online supplemental material

Fig. S1 shows additional analysis of the MS dataset. Fig. S2 shows representative images of HFF cells stained for paxillin and actin that were quantified in Fig. 3. Fig. S3 shows effects of treating cells with different doses of Src [i] on paxillin^{Y118} and Src^{Y416}. Fig. S4 shows additional quantification of immunofluorescence images in Fig. 6. Fig. S5 shows immunofluorescence images of NIH3T3 cells treated with FAK [i] or PF228. Table S1 displays a list of recombinant enzymes that were screened against FAK [i] or PF271. Tables S2 and S3 display proteins identified by MS upon FAK inhibition. The corresponding abundance value for each protein was normalized to total protein amount (Table S2) or vinculin abundance values (Table S3). Online supplemental material is available at http://www.jcb.org/cgi/content/full/jcb.201508080/DC1.

Acknowledgments

We thank A.P. Gilmore and P. Mendes for advice and discussions; D.H.J. Ng and J. Robertson for technical assistance with IAC isolations; S. Warwood and D. Knight for acquisition of MS data; J.N. Selley for bioinformatic support; P. March and S. Marsden for assistance with microscopy; and J. A. Askari, E.J. Koper, N.R. Paul, M.C. Jones, and P. Astudillo for technical assistance.

This work was supported by the Wellcome Trust (grant 092015 to M.J. Humphries) and a Wellcome Trust Institutional Strategic Support Fund award (grant 097820 to the University of Manchester). E.R. Horton is supported by a Biotechnology and Biological Sciences Research Council studentship from the Systems Biology Doctoral Training Centre. The mass spectrometers and microscopes used in this study were purchased with grants from the Biotechnology and Biological Sciences Research Council, Wellcome Trust, and the University of Manchester Strategic Fund.

The authors declare no competing financial interests.

Author contributions: J.D. Humphries and M.J. Humphries conceived the project; E.R. Horton performed the experiments and analyzed the data; B. Stutchbury performed FRAP experiments; E.R. Horton, J.D. Humphries, B. Stutchbury, G. Jacquemet, C. Ballestrem, S.T. Barry and M.J. Humphries interpreted the results; E.R. Horton, J.D. Humphries, and M.J. Humphries wrote the paper; all authors commented on the manuscript and approved the final version.

Submitted: 20 August 2015
Accepted: 6 January 2016

References

Ajeian, J.N., E.R. Horton, P. Astudillo, A. Byron, J.A. Askari, A. Millon-Frémillon, D. Knight, S.J. Kimber, M.J. Humphries, and J.D. Humphries. 2015. Proteomic analysis of integrin-associated complexes from mesenchymal stem cells. *Proteomics Clin. Appl.* http://dx.doi.org/10.1002/prca.201500033

Bachir, A.I., J. Zareno, K. Moissoglu, E.F. Plow, E. Gratton, and A.R. Horwitz. 2014. Integrin-associated complexes form hierarchically with variable stoichiometry in nascent adhesions. *Curr. Biol.* 24:1845–1853. http://dx.doi.org/10.1016/j.cub.2014.07.011

Bain, J., H. McLauchlan, M. Elliott, and P. Cohen. 2003. The specificities of protein kinase inhibitors: an update. *Biochem. J.* 371:199–204. http://dx.doi.org/10.1042/bj20021535

Ballestrem, C., N. Erez, J. Kirchner, Z. Kam, A. Bershadsky, and B. Geiger. 2006. Molecular mapping of tyrosine-phosphorylated proteins in focal adhesions using fluorescence resonance energy transfer. *J. Cell Sci.* 119:866–875. http://dx.doi.org/10.1242/jcs.02794

Bershadsky, A., A. Chausovsky, E. Becker, A. Lyubimova, and B. Geiger. 1996. Involvement of microtubules in the control of adhesion-dependent signal transduction. *Curr. Biol.* 6:1279–1289. http://dx.doi.org/10.1016/S0960-9822(02)70714-8

Brakebusch, C., and R. Fässler. 2003. The integrin-actin connection, an eternal love affair. *EMBO J.* 22:2324–2333. http://dx.doi.org/10.1093/emboj/cdg245

Brami-Cherrier, K., N. Gervasi, D. Arsenieva, K. Walkiewicz, M.C. Boutterin, A. Ortega, P.G. Leonard, B. Seantier, L. Gasmi, T. Bouceba, et al. 2014. FAK dimerization controls its kinase-dependent functions at focal adhesions. *EMBO J.* 33:356–370. http://dx.doi.org/10.1002/embj.201386399

Brunton, V.G., and M.C. Frame. 2008. Src and focal adhesion kinase as therapeutic targets in cancer. *Curr. Opin. Pharmacol.* 8:427–432. http://dx.doi.org/10.1016/j.coph.2008.06.012

Byron, A., M.R. Morgan, and M.J. Humphries. 2010. Adhesion signalling complexes. *Curr. Biol.* 20:R1063–R1067. http://dx.doi.org/10.1016/j.cub.2010.10.059

Byron, A., J.D. Humphries, S.E. Craig, D. Knight, and M.J. Humphries. 2012. Proteomic analysis of α4β1 integrin adhesion complexes reveals α-subunit-dependent protein recruitment. *Proteomics.* 12:2107–2114. http://dx.doi.org/10.1002/pmic.201100487

Byron, A., J.A. Askari, J.D. Humphries, G. Jacquemet, E.J. Koper, S. Warwood, C.K. Choi, M.J. Stroud, C.S. Chen, D. Knight, and M.J. Humphries. 2015. A proteomic approach reveals integrin activation state-dependent control of microtubule cortical targeting. *Nat. Commun.* 6:6135. http://dx.doi.org/10.1038/ncomms7135

Calalb, M.B., T.R. Polte, and S.K. Hanks. 1995. Tyrosine phosphorylation of focal adhesion kinase at sites in the catalytic domain regulates kinase activity: a role for Src family kinases. *Mol. Cell. Biol.* 15:954–963. http://dx.doi.org/10.1128/MCB.15.2.954

Chan, K.T., D.A. Bennin, and A. Huttenlocher. 2010. Regulation of adhesion dynamics by calpain-mediated proteolysis of focal adhesion kinase (FAK). *J. Biol. Chem.* 285:11418–11426. http://dx.doi.org/10.1074/jbc.M109.090746

Chautard, E., L. Ballut, N. Thierry-Mieg, and S. Ricard-Blum. 2009. MatrixDB, a database focused on extracellular protein-protein and protein-carbohydrate interactions. *Bioinformatics.* 25:690–691. http://dx.doi.org/10.1093/bioinformatics/btp025

Chen, Y., B. Lu, Q. Yang, C. Fearns, J.R. Yates, and J.-D. Lee. 2009. Combined integrin phosphoproteomic analyses and siRNA-based functional screening identified key regulators for cancer cell adhesion and migration. *Cancer Res.* 69:3713–3720. http://dx.doi.org/10.1158/0008-5472.CAN-08-2515

Choi, C.K., M. Vicente-Manzanares, J. Zareno, L.A. Whitmore, A. Mogilner, and A.R. Horwitz. 2008. Actin and α-actinin orchestrate the assembly and maturation of nascent adhesions in a myosin II motor-independent manner. *Nat. Cell Biol.* 10:1039–1050. http://dx.doi.org/10.1038/ncb1763

Chrzanowska-Wodnicka, M., and K. Burridge. 1996. Rho-stimulated contractility drives the formation of stress fibers and focal adhesions. *J. Cell Biol.* 133:1403–1415. http://dx.doi.org/10.1083/jcb.133.6.1403

Cline, M.S., M. Smoot, E. Cerami, A. Kuchinsky, N. Landys, C. Workman, R. Christmas, I. Avila-Campilo, M. Creech, B. Gross, et al. 2007. Integration of biological networks and gene expression data using Cytoscape. *Nat. Protoc.* 2:2366–2382. http://dx.doi.org/10.1038/nprot.2007.324

Davies, S.P., H. Reddy, M. Caivano, and P. Cohen. 2000. Specificity and mechanism of action of some commonly used protein kinase inhibitors. *Biochem. J.* 351:95–105. http://dx.doi.org/10.1042/bj3510095

Doyle, A.D., N. Carvajal, A. Jin, K. Matsumoto, and K.M. Yamada. 2015. Local 3D matrix microenvironment regulates cell migration through spatiotemporal dynamics of contractility-dependent adhesions. *Nat. Commun.* 6:8720. http://dx.doi.org/10.1038/ncomms9720

Dumbauld, D.W., K.E. Michael, S.K. Hanks, and A.J. García. 2010. Focal adhesion kinase-dependent regulation of adhesive forces involves vinculin recruitment to focal adhesions. *Biol. Cell.* 102:203–213. http://dx.doi.org/10.1042/BC20090104

Evans, E.A., and D.A. Calderwood. 2007. Forces and bond dynamics in cell adhesion. *Science.* 316:1148–1153. http://dx.doi.org/10.1126/science.1137592

Ezratty, E.J., M.A. Partridge, and G.G. Gundersen. 2005. Microtubule-induced focal adhesion disassembly is mediated by dynamin and focal adhesion kinase. *Nat. Cell Biol.* 7:581–590. http://dx.doi.org/10.1038/ncb1262

Gilmore, A.P., and L.H. Romer. 1996. Inhibition of focal adhesion kinase (FAK) signaling in focal adhesions decreases cell motility and proliferation. *Mol. Biol. Cell.* 7:1209–1224. http://dx.doi.org/10.1091/mbc.7.8.1209

Hennequin, L.F., J. Allen, J. Breed, J. Curwen, M. Fennell, T.P. Green, C. Lambert-van der Brempt, R. Morgentin, R.A. Norman, A. Olivier, et al.. 2006. N-(5-chloro-1,3-benzodioxol-4-yl)-7-[2-(4-methylpiperazin-1-yl)ethoxy]-5-(tetrahydro-2H-pyran-4-yloxy)quinazolin-4-amine, a novel, highly selective, orally available, dual-specific c-Src/Abl kinase inhibitor. *J. Med. Chem.* 49:6465–6488. http://dx.doi.org/10.1021/jm060434q

Hoffmann, J.-E., Y. Fermin, R.L. Stricker, K. Ickstadt, and E. Zamir. 2014. Symmetric exchange of multi-protein building blocks between stationary focal adhesions and the cytosol. *eLife.* 3:e02257. http://dx.doi.org/10.7554/eLife.02257

Holm, S. 1979. A simple sequentially rejective multiple test procedure. *Scand. J. Stat.* 6:65–70.

Horton, E.R., A. Byron, J.A. Askari, D.H.J. Ng, A. Millon-Frémillon, J. Robertson, E.J. Koper, N.R. Paul, S. Warwood, D. Knight, et al. 2015a. Definition of a consensus integrin adhesome and its dynamics during adhesion complex assembly and disassembly. *Nat. Cell Biol.* 17:1577–1587. http://dx.doi.org/10.1038/ncb3257

Horton, E.R., P. Astudillo, M.J. Humphries, and J.D. Humphries. 2015b. Mechanosensitivity of integrin adhesion complexes: role of the consensus adhesome. *Exp. Cell Res*. http://dx.doi.org/S0014-4827(15)30130-0

Hu, P., and B.-H. Luo. 2013. Integrin bi-directional signaling across the plasma membrane. *J. Cell. Physiol.* 228:306–312. http://dx.doi.org/10.1002/jcp.24154

Huang, I.H., C.T. Hsiao, J.C. Wu, R.F. Shen, C.Y. Liu, Y.K. Wang, Y.C. Chen, C.M. Huang, J.C. del Álamo, Z.F. Chang, et al. 2014. GEF-H1 controls focal adhesion signaling that regulates mesenchymal stem cell lineage commitment. *J. Cell Sci.* 127:4186–4200. http://dx.doi.org/10.1242/jcs.150227

Humphries, J.D., P. Wang, C. Streuli, B. Geiger, M.J. Humphries, and C. Ballestrem. 2007. Vinculin controls focal adhesion formation by direct interactions with talin and actin. *J. Cell Biol.* 179:1043–1057. http://dx.doi.org/10.1083/jcb.200703036

Humphries, J.D., A. Byron, M.D. Bass, S.E. Craig, J.W. Pinney, D. Knight, and M.J. Humphries. 2009. Proteomic analysis of integrin-associated complexes identifies RCC2 as a dual regulator of Rac1 and Arf6. *Sci. Signal.* 2:ra51. http://dx.doi.org/10.1126/scisignal.2000396

Humphries, J.D., N.R. Paul, M.J. Humphries, and M.R. Morgan. 2015. Emerging properties of adhesion complexes: what are they and what do they do? *Trends Cell Biol.* 25:388–397. http://dx.doi.org/10.1016/j.tcb.2015.02.008

Ilić, D., Y. Furuta, S. Kanazawa, N. Takeda, K. Sobue, N. Nakatsuji, S. Nomura, J. Fujimoto, M. Okada, and T. Yamamoto. 1995. Reduced cell motility and enhanced focal adhesion contact formation in cells from FAK-deficient mice. *Nature.* 377:539–544. http://dx.doi.org/10.1038/377539a0

Imamura, F., M. Mukai, M. Ayaki, and H. Akedo. 2000. Y-27632, an inhibitor of rho-associated protein kinase, suppresses tumor cell invasion via regulation of focal adhesion and focal adhesion kinase. *Jpn. J. Cancer Res.* 91:811–816. http://dx.doi.org/10.1111/j.1349-7006.2000.tb01018.x

Je, D.W., Y.M. O, Y.G. Ji, Y. Cho, and D.H. Lee. 2014. The inhibition of SRC family kinase suppresses pancreatic cancer cell proliferation, migration, and invasion. *Pancreas.* 43:768–776. http://dx.doi.org/10.1097/MPA.0000000000000103

Jones, M.C., J.D. Humphries, A. Byron, A. Millon-Frémillon, J. Robertson, N.R. Paul, D.H.J. Ng, J.A. Askari, and M.J. Humphries. 2015. Isolation of integrin-based adhesion complexes. *Curr. Protoc. Cell Biol.* 66:9.8.1–9.8: 15. http://dx.doi.org/10.1002/0471143030.cb0908s66

Juliano, R.L. 2002. Signal transduction by cell adhesion receptors and the cytoskeleton: functions of integrins, cadherins, selectins, and immunoglobulin-superfamily members. *Annu. Rev. Pharmacol. Toxicol.* 42:283–323. http://dx.doi.org/10.1146/annurev.pharmtox.42.090401.151133

Kim, L.C., L. Song, and E.B. Haura. 2009. Src kinases as therapeutic targets for cancer. *Nat. Rev. Clin. Oncol.* 6:587–595. http://dx.doi.org/10.1038/nrclinonc.2009.129

Kirchner, J., Z. Kam, G. Tzur, A.D. Bershadsky, and B. Geiger. 2003. Live-cell monitoring of tyrosine phosphorylation in focal adhesions following microtubule disruption. *J. Cell Sci.* 116:975–986. http://dx.doi.org/10.1242/jcs.00284

Kornberg, L., H.S. Earp, J.T. Parsons, M. Schaller, and R.L. Juliano. 1992. Cell adhesion or integrin clustering increases phosphorylation of a focal adhesion-associated tyrosine kinase. *J. Biol. Chem.* 267:23439–23442.

Kuo, J.C., X. Han, C.T. Hsiao, J.R. Yates III, and C.M. Waterman. 2011. Analysis of the myosin-II-responsive focal adhesion proteome reveals a role for β-Pix in negative regulation of focal adhesion maturation. *Nat. Cell Biol.* 13:383–393. http://dx.doi.org/10.1038/ncb2216

Kuo, J.C., X. Han, J.R. Yates III, and C.M. Waterman. 2012. Isolation of focal adhesion proteins for biochemical and proteomic analysis. *Methods Mol. Biol.* 757:297–323. http://dx.doi.org/10.1007/978-1-61779-166-6_19

Lawson, C., S.T. Lim, S. Uryu, X.L. Chen, D.A. Calderwood, and D.D. Schlaepfer. 2012. FAK promotes recruitment of talin to nascent adhesions to control cell motility. *J. Cell Biol.* 196:223–232. http://dx.doi.org/10.1083/jcb.201108078

Luo, M., X. Zhao, S. Chen, S. Liu, M.S. Wicha, and J.L. Guan. 2013. Distinct FAK activities determine progenitor and mammary stem cell characteristics. *Cancer Res.* 73:5591–5602. http://dx.doi.org/10.1158/0008-5472.CAN-13-1351

Maartens, A.P., and N.H. Brown. 2015. The many faces of cell adhesion during Drosophila muscle development. *Dev. Biol.* 401:62–74. http://dx.doi.org/10.1016/j.ydbio.2014.12.038

Meijering, E., O. Dzyubachyk, and I. Smal. 2012. Methods for cell and particle tracking. *Methods Enzymol.* 504:183–200. http://dx.doi.org/10.1016/B978-0-12-391857-4.00009-4

Mitchell, A., H.Y. Chang, L. Daugherty, M. Fraser, S. Hunter, R. Lopez, C. McAnulla, C. McMenamin, G. Nuka, S. Pesseat, et al. 2015. The InterPro protein families database: the classification resource after 15 years. *Nucleic Acids Res.* 43:D213–D221. http://dx.doi.org/10.1093/nar/gku1243

Mitra, S.K., and D.D. Schlaepfer. 2006. Integrin-regulated FAK-Src signaling in normal and cancer cells. *Curr. Opin. Cell Biol.* 18:516–523. http://dx.doi.org/10.1016/j.ceb.2006.08.011

Morgan, M.R., M.J. Humphries, and M.D. Bass. 2007. Synergistic control of cell adhesion by integrins and syndecans. *Nat. Rev. Mol. Cell Biol.* 8:957–969. http://dx.doi.org/10.1038/nrm2289

Nagoshi, Y., G. Yamamoto, T. Irie, and T. Tachikawa. 2006. Expression of FAK-related non-kinase (FRNK) coincides with morphological change in the early stage of cell adhesion. *Med. Mol. Morphol.* 39:154–160. http://dx.doi.org/10.1007/s00795-006-0325-8

Ng, D.H.J., J.D. Humphries, A. Byron, A. Millon-Frémillon, and M.J. Humphries. 2014. Microtubule-dependent modulation of adhesion complex composition. *PLoS One.* 9:e115213. http://dx.doi.org/10.1371/journal.pone.0115213

Oakes, P.W., Y. Beckham, J. Stricker, and M.L. Gardel. 2012. Tension is required but not sufficient for focal adhesion maturation without a stress fiber template. *J. Cell Biol.* 196:363–374. http://dx.doi.org/10.1083/jcb.201107042

Pasapera, A.M., I.C. Schneider, E. Rericha, D.D. Schlaepfer, and C.M. Waterman. 2010. Myosin II activity regulates vinculin recruitment to focal adhesions through FAK-mediated paxillin phosphorylation. *J. Cell Biol.* 188:877–890. http://dx.doi.org/10.1083/jcb.200906012

Perkins, D.N., D.J. Pappin, D.M. Creasy, and J.S. Cottrell. 1999. Probability-based protein identification by searching sequence databases using mass spectrometry data. *Electrophoresis.* 20:3551–3567. http://dx.doi.org/10.1002/(SICI)1522-2683(19991201)20:18<3551::AID-ELPS3551>3.0.CO;2-2

Plé, P.A., T.P. Green, L.F. Hennequin, J. Curwen, M. Fennell, J. Allen, C. Lambert-Van Der Brempt, and G. Costello. 2004. Discovery of a new class of anilinoquinazoline inhibitors with high affinity and specificity for the tyrosine kinase domain of c-Src. *J. Med. Chem.* 47:871–887. http://dx.doi.org/10.1021/jm030317k

Plotnikov, S.V., A.M. Pasapera, B. Sabass, and C.M. Waterman. 2012. Force fluctuations within focal adhesions mediate ECM-rigidity sensing to guide directed cell migration. *Cell.* 151:1513–1527. http://dx.doi.org/10.1016/j.cell.2012.11.034

Ren, X.D., W.B. Kiosses, D.J. Sieg, C.A. Otey, D.D. Schlaepfer, and M.A. Schwartz. 2000. Focal adhesion kinase suppresses Rho activity to promote focal adhesion turnover. *J. Cell Sci.* 113:3673–3678.

Richardson, A., and T. Parsons. 1996. A mechanism for regulation of the adhesion-associated proteintyrosine kinase pp125FAK. *Nature.* 380:538–540. http://dx.doi.org/10.1038/380538a0

Richardson, A., R.K. Malik, J.D. Hildebrand, and J.T. Parsons. 1997. Inhibition of cell spreading by expression of the C-terminal domain of focal adhesion kinase (FAK) is rescued by coexpression of Src or catalytically inactive FAK: a role for paxillin tyrosine phosphorylation. *Mol. Cell. Biol.* 17:6906–6914. http://dx.doi.org/10.1128/MCB.17.12.6906

Robertson, J., G. Jacquemet, A. Byron, M.C. Jones, S. Warwood, J.N. Selley, D. Knight, J.D. Humphries, and M.J. Humphries. 2015. Defining the phospho-adhesome through the phosphoproteomic analysis of integrin signalling. *Nat. Commun.* 6:6265. http://dx.doi.org/10.1038/ncomms7265

Sánchez-Bailón, M.P., A. Calcabrini, D. Gómez-Domínguez, B. Morte, E. Martín-Forero, G. Gómez-López, A. Molinari, K.U. Wagner, and J. Martín-Pérez. 2012. Src kinases catalytic activity regulates proliferation, migration and invasiveness of MDA-MB-231 breast cancer cells. *Cell. Signal.* 24:1276–1286. http://dx.doi.org/10.1016/j.cellsig.2012.02.011

Schaller, M.D., and J.T. Parsons. 1995. pp125FAK-dependent tyrosine phosphorylation of paxillin creates a high-affinity binding site for Crk. *Mol. Cell. Biol.* 15:2635–2645. http://dx.doi.org/10.1128/MCB.15.5.2635

Schaller, M.D., C.A. Borgman, B.S. Cobb, R.R. Vines, A.B. Reynolds, and J.T. Parsons. 1992. pp125FAK a structurally distinctive protein-tyrosine kinase associated with focal adhesions. *Proc. Natl. Acad. Sci. USA.* 89:5192–5196. http://dx.doi.org/10.1073/pnas.89.11.5192

Schaller, M.D., J.D. Hildebrand, J.D. Shannon, J.W. Fox, R.R. Vines, and J.T. Parsons. 1994. Autophosphorylation of the focal adhesion kinase, pp125FAK, directs SH2-dependent binding of pp60src. *Mol. Cell. Biol.* 14:1680–1688. http://dx.doi.org/10.1128/MCB.14.3.1680

Schiller, H.B., C.C. Friedel, C. Boulegue, and R. Fässler. 2011. Quantitative proteomics of the integrin adhesome show a myosin II-dependent recruitment of LIM domain proteins. *EMBO Rep.* 12:259–266. http://dx.doi.org/10.1038/embor.2011.5

Schiller, H.B., M.R. Hermann, J. Polleux, T. Vignaud, S. Zanivan, C.C. Friedel, Z. Sun, A. Raducanu, K.-E. Gottschalk, M. Théry, et al. 2013. β1- and αv-class integrins cooperate to regulate myosin II during rigidity sensing of fibronectin-based microenvironments. *Nat. Cell Biol.* 15:625–636. http://dx.doi.org/10.1038/ncb2747

Schindelin, J., I. Arganda-Carreras, E. Frise, V. Kaynig, M. Longair, T. Pietzsch, S. Preibisch, C. Rueden, S. Saalfeld, B. Schmid, et al. 2012. Fiji: an open-source platform for biological-image analysis. *Nat. Methods.* 9:676–682. http://dx.doi.org/10.1038/nmeth.2019

Schober, M., S. Raghavan, M. Nikolova, L. Polak, H.A. Pasolli, H.E. Beggs, L.F. Reichardt, and E. Fuchs. 2007. Focal adhesion kinase modulates tension signaling to control actin and focal adhesion dynamics. *J. Cell Biol.* 176:667–680. http://dx.doi.org/10.1083/jcb.200608010

Serrels, A., I.R.J. Macpherson, T.R.J. Evans, F.Y. Lee, E.A. Clark, O.J. Sansom, G.H. Ashton, M.C. Frame, and V.G. Brunton. 2006. Identification of potential biomarkers for measuring inhibition of Src kinase activity in colon cancer cells following treatment with dasatinib. *Mol. Cancer Ther.* 5:3014–3022. http://dx.doi.org/10.1158/1535-7163.MCT-06-0382

Serrels, A., K. McLeod, M. Canel, A. Kinnaird, K. Graham, M.C. Frame, and V.G. Brunton. 2012. The role of focal adhesion kinase catalytic activity on the proliferation and migration of squamous cell carcinoma cells. *Int. J. Cancer.* 131:287–297. http://dx.doi.org/10.1002/ijc.26351

Shevchenko, A., M. Wilm, O. Vorm, and M. Mann. 1996. Mass spectrometric sequencing of proteins silver-stained polyacrylamide gels. *Anal. Chem.* 68:850–858. http://dx.doi.org/10.1021/ac950914h

Sieg, D.J., D. Ilić, K.C. Jones, C.H. Damsky, T. Hunter, and D.D. Schlaepfer. 1998. Pyk2 and Src-family protein-tyrosine kinases compensate for the loss of FAK in fibronectin-stimulated signaling events but Pyk2 does not fully function to enhance FAK$^-$ cell migration. *EMBO J.* 17:5933–5947. http://dx.doi.org/10.1093/emboj/17.20.5933

Sieg, D.J., C.R. Hauck, and D.D. Schlaepfer. 1999. Required role of focal adhesion kinase (FAK) for integrin-stimulated cell migration. *J. Cell Sci.* 112:2677–2691.

Sieg, D.J., C.R. Hauck, D. Ilić, C.K. Klingbeil, E. Schaefer, C.H. Damsky, and D.D. Schlaepfer. 2000. FAK integrates growth-factor and integrin signals to promote cell migration. *Nat. Cell Biol.* 2:249–256. http://dx.doi.org/10.1038/35010517

Slack, J.K., R.B. Adams, J.D. Rovin, E.A. Bissonette, C.E. Stoker, and J.T. Parsons. 2001. Alterations in the focal adhesion kinase/Src signal transduction pathway correlate with increased migratory capacity of prostate carcinoma cells. *Oncogene.* 20:1152–1163. http://dx.doi.org/10.1038/sj.onc.1204208

Slack-Davis, J.K., K.H. Martin, R.W. Tilghman, M. Iwanicki, E.J. Ung, C. Autry, M.J. Luzzio, B. Cooper, J.C. Kath, W.G. Roberts, and J.T. Parsons. 2007. Cellular characterization of a novel focal adhesion kinase inhibitor. *J. Biol. Chem.* 282:14845–14852. http://dx.doi.org/10.1074/jbc.M606695200

Stokes, J.B., S.J. Adair, J.K. Slack-Davis, D.M. Walters, R.W. Tilghman, E.D. Hershey, B. Lowrey, K.S. Thomas, A.H. Bouton, R.F. Hwang, et al. 2011. Inhibition of focal adhesion kinase by PF-562,271 inhibits the growth and metastasis of pancreatic cancer concomitant with altering the tumor microenvironment. *Mol. Cancer Ther.* 10:2135–2145. http://dx.doi.org/10.1158/1535-7163.MCT-11-0261

Sulzmaier, F.J., C. Jean, and D.D. Schlaepfer. 2014. FAK in cancer: mechanistic findings and clinical applications. *Nat. Rev. Cancer.* 14:598–610. http://dx.doi.org/10.1038/nrc3792

Tanjoni, I., C. Walsh, S. Uryu, A. Tomar, J.-O. Nam, A. Mielgo, S.-T. Lim, C. Liang, M. Koenig, C. Sun, et al. 2010. PND-1186 FAK inhibitor selectively promotes tumor cell apoptosis in three-dimensional environments. *Cancer Biol. Ther.* 9:764–777. http://dx.doi.org/10.4161/cbt.9.10.11434

Vizcaíno, J.A., R.G. Côté, A. Csordas, J.A. Dianes, A. Fabregat, J.M. Foster, J. Griss, E. Alpi, M. Birim, J. Contell, et al. 2013. The PRoteomics IDEntifications (PRIDE) database and associated tools: status in 2013. *Nucleic Acids Res.* 41:D1063–D1069. http://dx.doi.org/10.1093/nar/gks1262

Wahl, S.M., G.M. Feldman, and J.B. McCarthy. 1996. Regulation of leukocyte adhesion and signaling in inflammation and disease. *J. Leukoc. Biol.* 59:789–796.

Wang, H.B., M. Dembo, S.K. Hanks, and Y. Wang. 2001. Focal adhesion kinase is involved in mechanosensing during fibroblast migration. *Proc. Natl. Acad. Sci. USA.* 98:11295–11300. http://dx.doi.org/10.1073/pnas.201201198

Webb, D.J., K. Donais, L.A. Whitmore, S.M. Thomas, C.E. Turner, J.T. Parsons, and A.F. Horwitz. 2004. FAK-Src signalling through paxillin, ERK and MLCK regulates adhesion disassembly. *Nat. Cell Biol.* 6:154–161. http://dx.doi.org/10.1038/ncb1094

Westhoff, M.A., B. Serrels, V.J. Fincham, M.C. Frame, and N.O. Carragher. 2004. SRC-mediated phosphorylation of focal adhesion kinase couples actin and adhesion dynamics to survival signaling. *Mol. Cell. Biol.* 24:8113–8133. http://dx.doi.org/10.1128/MCB.24.18.8113-8133.2004

Winograd-Katz, S.E., R. Fässler, B. Geiger, and K.R. Legate. 2014. The integrin adhesome: from genes and proteins to human disease. *Nat. Rev. Mol. Cell Biol.* 15:273–288. http://dx.doi.org/10.1038/nrm3769

Wu, J., T. Vallenius, K. Ovaska, J. Westermarck, T.P. Mäkelä, and S. Hautaniemi. 2009. Integrated network analysis platform for protein-protein interactions. *Nat. Methods.* 6:75–77. http://dx.doi.org/10.1038/nmeth.1282

Yue, J., M. Xie, X. Gou, P. Lee, M.D. Schneider, and X. Wu. 2014. Microtubules regulate focal adhesion dynamics through MAP4K4. *Dev. Cell.* 31:572–585. http://dx.doi.org/10.1016/j.devcel.2014.10.025

Zaidel-Bar, R., and B. Geiger. 2010. The switchable integrin adhesome. *J. Cell Sci.* 123:1385–1388. http://dx.doi.org/10.1242/jcs.066183

Zaidel-Bar, R., S. Itzkovitz, A. Ma'ayan, R. Iyengar, and B. Geiger. 2007. Functional atlas of the integrin adhesome. *Nat. Cell Biol.* 9:858–867. http://dx.doi.org/10.1038/ncb0807-858